Volume 0 (1981), Number 0 pp. 1–24 COMPUTER GRAPHICS *forum*

The State of the Art in Vortex Extraction

Tobias Günther[1] and Holger Theisel[2]

[1]ETH Zürich, Switzerland
[2]University of Magdeburg, Germany

Abstract

Vortices are commonly understood as rotating motions in fluid flows. The analysis of vortices plays an important role in numerous scientific applications, such as in engineering, meteorology, oceanology, medicine and many more. The successful analysis consists of three steps: vortex definition, extraction and visualization. All three have a long history, and the early themes and topics from the 70s survived to this day, namely the identification of vortex cores, their extent and the choice of suitable reference frames. This paper provides an overview over the advances that have been made in the last forty years. We provide sufficient background on differential vector field calculus, extraction techniques like critical point search and the parallel vectors operator, and we introduce the notion of reference frame invariance. We explain the most important region-based and line-based methods, integration-based and geometry-based approaches, recent objective techniques, the selection of reference frames by means of flow decompositions, as well as a recent local optimization-based technique. We point out relationships between the various approaches, classify the literature and identify open problems and challenges for future work.

This is the authors preprint. The definitive version is available at http://onlinelibrary.wiley.com/.

1. Introduction

Vortex extraction belongs to the most important and similarly most challenging aspects of fluid flow analysis. Vortices are commonly understood as rotational or spiraling movements of particles around a common coreline, which can be seen only if the flow is viewed in the right reference frame [Lug79, Rob91]. Vortices play a significant role in many engineering problems, for instance in aircraft navigation during nose-up or roll of a jet [KH97], where vortices may reduce lift. Other examples are swirl and tumble motion in gas engines [GLT*07], and turbomachinery [RP96], where flows exhibit fully developed turbulence, strong shear and are constrained in curved channels of complex geometry. Recently, vortices have drawn more attention in medical applications, such as in 4D PC-MRI cardiac blood flow [KGP*13] and in risk assessment of cerebral aneurysms [OJCJP16]. Vortices are explored in the oceans in form of eddies [CSSdS07] and in the atmosphere in the search for hurricanes [Lug83]. Also, vortices in the atmosphere of other planets such as Jupiter shifted into focus [HH16]. Fig. 1 depicts vortices in the wake of an air plane and in the clouds behind an island.

Despite their relevance in practice, the analysis tools are limited in their capabilities. Most techniques require the flow to be incompressible and the identification of vortices becomes particularly difficult in time-dependent flows, which is in the top list of long-standing and open challenges of flow visualization. Traditionally, flow visualization is divided into four categories.

- *Direct methods* use primitives to directly encode properties of the data, e.g., arrow plots pointing in the flow direction. Glyphs can be used to encode multiple attributes [BKC*13], which is suitable for multi-variate data visualization. While they are widely and successfully applied in 2D, their utility is limited when they are spatially embedded in 3D due to the arising occlusion.
- *Geometry-based methods* use geometric primitives such as flow aligning lines and surfaces to represent a flow. A comprehensive overview of geometry-based approaches is given by McLoughlin et al. [MLP*10]. Recent reports focused on surface-based [ELC*12] and illustrative flow visualization [BCP*12].
- *Texture-based methods* are sometimes also referred to as dense methods, since they densely encode data using textures. These methods are predominantly used in 2D and on 2D manifolds, again due to the occlusion problems. A famous example is the line integral convolution (LIC) [CL93]. More details on texture-based methods are found in [LHD*04] and [LEG*08].
- In *feature-based methods*, the term *feature* is often reserved for structures that are contained in vector field topology [HH91]. The essence of these methods is to partition and compactly describe the flow as a set of areas with coherent behavior. More information on the extraction and tracking of feature is compiled in [PVH*03]. More recent reports summarize the efforts in topology-based [HLH*16, LHZP07] and specifically unsteady topology-based [PPF*11] flow visualization.

Vortex extraction resides in the area of feature-based methods,

Figure 1: Examples of real-world air flows. Left: wake vortex study of an agricultural plane (image from the NASA Langley Research Center), right: clouds off the Chilean coast near the Juan Fernandez Islands form a von-Kármán vortex street (by Bob Cahalan, NASA Goddard Space Flight Center). Both images are in public domain.

though there are some synergies with geometry-based techniques for integration-based extraction and visualization. Over the past years, several new challenges emerged in the scientific disciplines that scientific visualization supports, which led to an increased demand for research on specific challenges, such as time-dependent flows, multi-fields, higher-dimensional flows, large-scale and in-situ visualization, ensembles and uncertainty. Vortex extraction is a relevant subject in all of these new challenges.

This paper is aimed to be an entry point for new researchers and a comprehensive overview for the senior ones. First, we cover in Section 2 the basic differential properties and principles that most vortex extraction techniques are based on. Further, we outline the most relevant extraction techniques, i.e., critical point search and parallel vectors. Section 3 introduces the concept of reference frame invariance, which allows us to understand when vortex extraction techniques will fail. In Section 4, we provide an overview and classify vortex extraction techniques. Afterwards, we proceed with numerous vortex definitions throughout Section 5. Topic-wise, we cover traditional region-based and line-based techniques, geometric and integration-based methods, objective techniques, flow decompositions and reference frame selection, including an optimization-based approach. Afterwards, we look into topics such as the determination of a vortex boundary, vorticity transport, vortex verification and vortex visualization. Finally, Section 6 concludes and outlines directions for future research.

1.1. Notation

Throughout the paper, we denote scalars by italic lowercase letters such as s, column vectors with bold lowercase letters such as $\mathbf{v}$, and matrices with bold uppercase letters such as $\mathbf{J}$. Formally, we denote coordinates in space as $\mathbf{x}$ and coordinates in space-time with a bar as $\bar{\mathbf{x}}$. A squared bracket indicates a differences between 2D and 3D:

$$\mathbf{x} = \begin{pmatrix} x \\ y \\ [z] \end{pmatrix} \in D\,, \quad \bar{\mathbf{x}} = \begin{pmatrix} x \\ y \\ [z] \\ t \end{pmatrix} \in D \times T \tag{1}$$

where the spatial domain D is a subset of the n-dimensional ($n = 2,3$) Euclidean space $\mathbb{E}^n$, i.e., $D \subset \mathbb{E}^n$ and T is a time interval. Later, we use the space-time concept to represent the state of a particle in a time-dependent flow, including both its location in space and in time.

We define function ap to transform the anti-symmetric part of a matrix to a scalar/vector. In 2D, $ap(\mathbf{M}) = \frac{1}{2}(m_{1,2} - m_{2,1})$. In 3D, $ap(\mathbf{M}) = \frac{1}{2}(m_{3,2} - m_{2,3}\,, m_{1,3} - m_{3,1}\,, m_{2,1} - m_{1,2})^{\mathrm{T}}$ where $m_{i,j}$ refer to the elements of the matrix $\mathbf{M}$. The inverse of ap is the function sk that transforms a scalar/vector into an antisymmetric matrix. In 2D and 3D, we have:

$$2D:\ sk(\alpha) = \begin{pmatrix} 0 & \alpha \\ -\alpha & 0 \end{pmatrix}, \quad 3D:\ sk\begin{pmatrix} \alpha \\ \beta \\ \gamma \end{pmatrix} = \begin{pmatrix} 0 & -\gamma & \beta \\ \gamma & 0 & -\alpha \\ -\beta & \alpha & 0 \end{pmatrix} \tag{2}$$

Further, we denote the trace of matrix $\mathbf{M}$ as $tr(\mathbf{M})$, the determinant as $det(\mathbf{M})$ and the Euclidean norm as $\|\mathbf{M}\| = \sqrt{tr(\mathbf{M}\mathbf{M}^{\mathrm{T}})}$.

2. Background

The following section briefly introduces the most important concepts that are used in the literature on vortex extraction.

2.1. Steady and Unsteady Vector Fields

First of all, we distinguish between *steady* and *unsteady* flows.

Steady Vector Field. A steady vector field is not changing over time and is formally given as a time-independent map $\mathbf{v}(\mathbf{x}) = \mathbf{v}(x, y\,[, z]) : D \to D$.

$$2D:\ \mathbf{v}(x,y) = \begin{pmatrix} u(x,y) \\ v(x,y) \end{pmatrix} \qquad 3D:\ \mathbf{v}(x,y,z) = \begin{pmatrix} u(x,y,z) \\ v(x,y,z) \\ w(x,y,z) \end{pmatrix} \tag{3}$$

where $u, v[, w]$ denote the direction components. Steady flows are used to describe instantaneous fields, or generally fields that do not change over time. An example for an instantaneous field is a magnetic field. Even though it might change over time, we are usually interested in a single time slice.

Unsteady Vector Field. An unsteady vector field, on the other hand, varies over time, and thus, it is given as a time-dependent map $\mathbf{v}(\mathbf{x},t) = \mathbf{v}(x, y, [z,]\, t) : D \times T \to D$. In 2D and 3D, we have:

$$2D:\ \mathbf{v}(x,y,t) = \begin{pmatrix} u(x,y,t) \\ v(x,y,t) \end{pmatrix} \qquad 3D:\ \mathbf{v}(x,y,z,t) = \begin{pmatrix} u(x,y,z,t) \\ v(x,y,z,t) \\ w(x,y,z,t) \end{pmatrix} \tag{4}$$

Most physical processes are subject to temporal variation, including the motion of air and liquids. In such an unsteady flow, vortices move. Their robust tracking over time is among the most challenging aspects of vortex extraction.

Streamlines. In a *steady* flow, the trajectory $\mathbf{x}(\tau)$ of a tracer particle is called a *streamline*. For a given seed point $\mathbf{x}_0$, the streamline

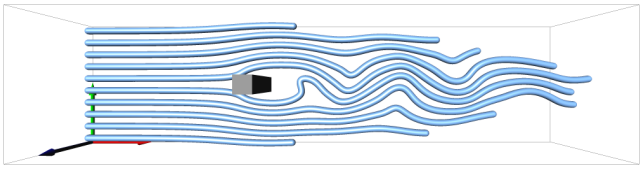

(a) **Streamlines**: trajectories in a single time slice.

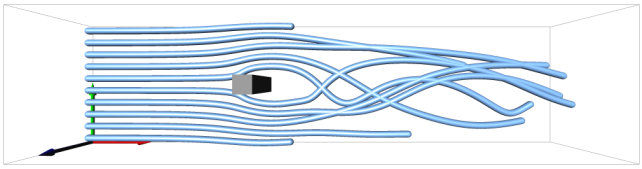

(b) **Pathlines**: trajectories of tracer particles, advancing in time.

Figure 2: Examples of integral curves in unsteady flow. This illustration was provided in [Gün16].

is computed as the solution to the autonomous ordinary differential equation (ODE):

$$\frac{\mathrm{d}}{\mathrm{d}\tau}\mathbf{x}(\tau) = \mathbf{v}(\mathbf{x}(\tau)) \quad \text{with} \quad \mathbf{x}(0) = \mathbf{x}_0. \tag{5}$$

An example for streamlines in unsteady data are the instantaneous field lines of unsteady magnetic fields. Fig. 2a shows streamlines in the flow around an obstacle.

Pathlines. In an *unsteady* flow, the trajectory $\mathbf{x}(t)$ of a tracer particle is called a *pathline*. For a given seed point $\mathbf{x}_0$ and seed time t_0, it is the solution to the ODE:

$$\frac{\mathrm{d}}{\mathrm{d}t}\mathbf{x}(t) = \mathbf{v}(\mathbf{x}(t),t) \quad \text{with} \quad \mathbf{x}(t_0) = \mathbf{x}_0. \tag{6}$$

By interpreting a time-dependent vector field as an autonomous system in space-time, it can be written as an $(n+1)$-dimensional steady field:

$$2D:\ \bar{\mathbf{p}}(x,y,t) = \begin{pmatrix} u(x,y,t) \\ v(x,y,t) \\ 1 \end{pmatrix}, \quad 3D:\ \bar{\mathbf{p}}(x,y,z,t) = \begin{pmatrix} u(x,y,z,t) \\ v(x,y,z,t) \\ w(x,y,z,t) \\ 1 \end{pmatrix}. \tag{7}$$

Here, an infinite number of pathlines passes through each point in the spatial domain, depending on the seed time of the curve. Fig. 2b gives an example.

2.2. Derivatives and Differential Properties of Vector Fields

Most vortex definitions are characterized by means of differential properties of the observed vector field. This section introduces the most relevant properties. We denote the partial derivatives of a vector field $\mathbf{v}$ as:

$$\mathbf{v}_x = \frac{\partial \mathbf{v}}{\partial x}, \quad \mathbf{v}_y = \frac{\partial \mathbf{v}}{\partial y}, \quad \left[\mathbf{v}_z = \frac{\partial \mathbf{v}}{\partial z},\right] \quad \mathbf{v}_t = \frac{\partial \mathbf{v}}{\partial t}. \tag{8}$$

Note that for steady flows $\mathbf{v}_t = \mathbf{0}$.

Nabla Operator. The Nabla operator ∇ is a symbol that simplifies the notation of several derived differential quantities. It is a vector that contains the partial derivative symbols with respect to the spatial dimensions:

$$\nabla = \left(\frac{\partial}{\partial x}, \frac{\partial}{\partial y}\left[, \frac{\partial}{\partial z}\right]\right)^{\mathrm{T}} \tag{9}$$

Divergence. The divergence $\nabla \cdot \mathbf{v}$ of a steady or unsteady flow $\mathbf{v}(x, y[, z, t]) = (u, v[, w])^{\mathrm{T}}$ is a scalar field that characterizes the change in volume of a virtual finite-sized sphere that is advected with the flow. The divergence is given as:

$$\nabla \cdot \mathbf{v} = \frac{\partial u}{\partial x} + \frac{\partial v}{\partial y}\left[+\frac{\partial w}{\partial z}\right] = u_x + v_y\,[+w_z] \tag{10}$$

If the volume increases the divergence is positive; if it decreases the divergence is negative. If the volume remains constant, even though the shape of the sphere might deform, the divergence is zero. If a flow has zero divergence everywhere in the domain, the flow is referred to as *divergence-free* or incompressible. The compressibility of a fluid depends on its molecular composition. Tightly packed fluids such as water are often modeled as incompressible. Since gases can easily be packed tighter under pressure, they are highly compressible and not divergence-free.

Curl. The curl $\nabla \times \mathbf{v}$ of a steady 3D vector field $\mathbf{v}(x, y, z) = (u, v, w)^{\mathrm{T}}$ is a vector field that indicates how the flow swirls at a certain point. It is defined as:

$$\nabla \times \mathbf{v} = \begin{pmatrix} w_y - v_z \\ u_z - w_x \\ v_x - u_y \end{pmatrix} \tag{11}$$

When a virtual finite-sized particle is advected with the flow, it might spin. The axis around which it spins is parallel to the curl vector and the curl's magnitude corresponds to half the angular speed of the rotation. A vector field in which the curl is the zero vector everywhere in the domain is called *curl-free* or irrotational.

Harmonic Flow. A vector field that is both divergence-free and curl-free is called *harmonic*.

$$\mathbf{v} \text{ is harmonic} \quad \Leftrightarrow \quad \nabla \cdot \mathbf{v} = 0 \ \wedge \ \nabla \times \mathbf{v} = \mathbf{0} \tag{12}$$

Harmonic flows play a role in flow decompositions, such as the Helmholtz-Hodge decomposition [BNPB13].

Jacobian. The spatial Jacobian $\mathbf{J} = \nabla\mathbf{v} = (\mathbf{v}_x, \mathbf{v}_y[, \mathbf{v}_z])$ is an $n \times n$ matrix that contains a first-order description of how the flow behaves locally around a given location. The space-time Jacobian $\bar{\mathbf{J}}$ is an $(n+1) \times (n+1)$ matrix that additionally contains the temporal derivative. It is defined as:

$$\bar{\mathbf{J}} = \nabla\bar{\mathbf{p}} = \begin{pmatrix} \mathbf{J} & \mathbf{v}_t \\ \mathbf{0}^{\mathrm{T}} & 0 \end{pmatrix}. \tag{13}$$

In a steady flow, the eigenvalues and eigenvectors of the Jacobian $\mathbf{J}$ are of great interest to characterize isolated first-order critical points [HH89, HH91, Wei08], i.e., locations at which $\mathbf{v}(\mathbf{x}) = \mathbf{0}$. We denote the eigenvectors of $\mathbf{J}$ as $\mathbf{e}_1, \mathbf{e}_2[, \mathbf{e}_3]$, respectively. The eigenvectors will play a significant role for the definition of vortex concepts. Many region-based vortex extraction methods are based on

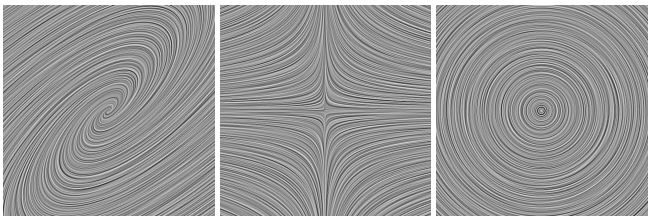

(a) Jacobian $\mathbf{J}$ (b) Strain rate tensor $\mathbf{S}$ (c) Vorticity tensor $\mathbf{\Omega}$

Figure 3: Decomposition of the Jacobian $\mathbf{J}$ into symmetric part $\mathbf{S}$ and anti-symmetric part $\mathbf{\Omega}$. Each tensor is visualized with a LIC [CL93], using $\mathbf{v} = \mathbf{J}\mathbf{x}$, $\mathbf{v} = \mathbf{S}\mathbf{x}$ and $\mathbf{v} = \mathbf{\Omega}\mathbf{x}$, respectively.

the decomposition of the Jacobian $\mathbf{J}$ into $\mathbf{J} = \mathbf{S} + \mathbf{\Omega}$, with

$$\mathbf{S} = \frac{\mathbf{J} + \mathbf{J}^{\mathrm{T}}}{2} \qquad \mathbf{\Omega} = \frac{\mathbf{J} - \mathbf{J}^{\mathrm{T}}}{2} \tag{14}$$

where the symmetric matrix $\mathbf{S}$ is called the *strain rate tensor* and the anti-symmetric matrix $\mathbf{\Omega}$ is called the *vorticity tensor*. Fig. 3 illustrates the components of this decomposition for the simple linear vector field $\mathbf{v} = (x + y, -x - \frac{2}{5}y)^{\mathrm{T}}$.

Jacobian Invariants. In 3D flows, the eigenvalues of the Jacobian $\mathbf{J}$ satisfy:

$$\lambda^3 - P\lambda^2 + Q\lambda - R = 0 \tag{15}$$

Thereby, P, Q and R are tensor invariants, since they remain the same in any basis. Here, they are defined as:

$$P = tr(\mathbf{J}) = \nabla \cdot \mathbf{v} \tag{16}$$

$$Q = \frac{1}{2}\left(P^2 - tr(\mathbf{J}^2)\right) \tag{17}$$

$$= \frac{1}{2}(\|\mathbf{\Omega}\|^2 - \|\mathbf{S}\|^2) + \frac{1}{2}(\nabla \cdot \mathbf{v})^2 \tag{18}$$

$$R = det(\mathbf{J}) \tag{19}$$

using $\mathbf{J} = \mathbf{S} + \mathbf{\Omega}$ from Eq. (14), and $\|\cdot\|$ denotes the Euclidean norm of a tensor. Some of the most-established vortex definitions are based on the invariants of the Jacobian matrix, as we will see later. Note that for 2D flows, there are only two invariants:

$$P = tr(\mathbf{J}) = \nabla \cdot \mathbf{v} \tag{20}$$

$$Q = \frac{1}{2}\left(P^2 - tr(\mathbf{J}^2)\right) = det(\mathbf{J}) \tag{21}$$

Acceleration. The acceleration of a particle in space is

$$\frac{D\mathbf{v}}{Dt} = \mathbf{a} = \mathbf{J} \cdot \mathbf{v} + \mathbf{v}_t \ , \tag{22}$$

and the acceleration in space-time is $\bar{\mathbf{a}} = \bar{\mathbf{J}}\,\bar{\mathbf{p}}$. Note that $\bar{\mathbf{a}} = \begin{pmatrix} \mathbf{a} \\ 0 \end{pmatrix}$.

Feature Flow Field. The feature flow field is a derived vector field that has several fundamental properties. Originally, it was defined in space-time as $\bar{\mathbf{f}}$ [TS03]. The most important observations are:

1. Given an unsteady 2D flow $\bar{\mathbf{p}}$ in space-time as in Eq. (7), the feature flow field $\bar{\mathbf{f}}$ points in space-time into the direction in which neither u nor v will change:

   $$\bar{\mathbf{f}} = \nabla u \times \nabla v \tag{23}$$

   Note that the cross product assures that $\bar{\mathbf{f}}$ is orthogonal to both ∇u and ∇v. From this, it can be shown that $\bar{\mathbf{f}}$ is divergence-free. For $n = 2$, this gives [TS03]:

   $$\bar{\mathbf{f}} = \begin{pmatrix} det(\mathbf{v}_y, \mathbf{v}_t) \\ det(\mathbf{v}_t, \mathbf{v}_x) \\ det(\mathbf{v}_x, \mathbf{v}_y) \end{pmatrix} \ , \ \mathbf{f} = \frac{1}{det(\mathbf{v}_x, \mathbf{v}_y)} \begin{pmatrix} det(\mathbf{v}_y, \mathbf{v}_t) \\ det(\mathbf{v}_t, \mathbf{v}_x) \end{pmatrix}. \tag{24}$$

   Similarly, for $n = 3$ we have [WSTH07]:

   $$\bar{\mathbf{f}} = \begin{pmatrix} -det(\mathbf{v}_y, \mathbf{v}_z, \mathbf{v}_t) \\ det(\mathbf{v}_z, \mathbf{v}_t, \mathbf{v}_x) \\ -det(\mathbf{v}_t, \mathbf{v}_x, \mathbf{v}_y) \\ det(\mathbf{v}_x, \mathbf{v}_y, \mathbf{v}_z) \end{pmatrix}, \ \mathbf{f} = \frac{1}{det(\mathbf{v}_x, \mathbf{v}_y, \mathbf{v}_z)} \begin{pmatrix} -det(\mathbf{v}_y, \mathbf{v}_z, \mathbf{v}_t) \\ det(\mathbf{v}_z, \mathbf{v}_t, \mathbf{v}_x) \\ -det(\mathbf{v}_t, \mathbf{v}_x, \mathbf{v}_y) \end{pmatrix}. \tag{25}$$

   Note that a division by the last component of $\bar{\mathbf{f}}$ gives a variant of the feature field that is named $\mathbf{f}$, which is defined in space only, see Eqs. (24)–(25). The feature flow field can also be computed as, cf. [Gün16]:

   $$\mathbf{f} = -\mathbf{J}^{-1}\,\mathbf{v}_t \ . \tag{26}$$

   Note that $\mathbf{f}$ can only be computed if $\mathbf{J}$ is non-singular. When seeding a particle at a critical point, the tangent curves of $\mathbf{f}$ will follow the paths of critical points in space-time [TS03].
2. Let $\mathbf{e}_1, \mathbf{e}_2, [\mathbf{e}_3]$ be the eigenvectors of Jacobian $\mathbf{J}$. The space-time Jacobian $\bar{\mathbf{J}}$ has eigenvectors $\begin{pmatrix} \mathbf{e}_1 \\ 0 \end{pmatrix}, \begin{pmatrix} \mathbf{e}_2 \\ 0 \end{pmatrix}, \left[\begin{pmatrix} \mathbf{e}_3 \\ 0 \end{pmatrix}\right], \begin{pmatrix} \mathbf{f} \\ 1 \end{pmatrix}$, where $\mathbf{f}$ has the corresponding eigenvalue 0. Thus, the feature flow field is also an eigenvector with real-valued eigenvalue, which plays a role for constructing space-time planes in which no swirling motion occurs [WSTH07].

As shown later, the feature flow field $\mathbf{v}$ can be used to derive vortex extractors for unsteady flows.

2.3. Vector Field Topology

Topology-based visualization aims for compact descriptions of vector fields. This includes the extraction of features and the segmentation of the domain into regions of coherent asymptotic behavior. One of the these features are centers of rotating motion, i.e., vortices. We briefly review vector field topology, since many vortex extraction techniques (especially in 2D), eventually reduce to an exercise in the extraction of the vector field topology of a derived vector field. This aside, topological methods received much attention and became a very active research area. Among others, they spurred work to smooth [WJE01], simplify [TSH00], compress [LRR00, TRS03], model [The02, WTHS04b] or edit [CML*07] vector fields. In the following, we briefly dive into the basics of vector field topology. We refer to Heine et al. [HLH*16], Scheuermann and Tricoche [ST05], and Weinkauf [Wei08] for a comprehensive introduction into topology-based methods.

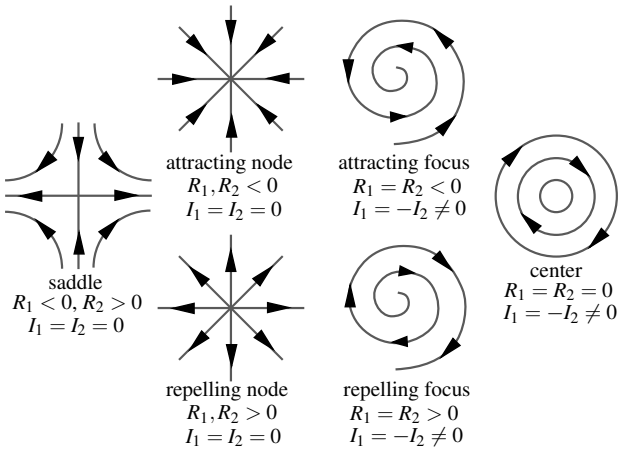

Figure 4: Types of critical points in 2D steady vector fields (based on [HH89]). R_1 and R_2 denote the real parts of the eigenvalues and I_1 and I_2 the imaginary parts. Note that the presence of imaginary parts (right half) relates to vortical behavior.

Definition of First-Order Critical Points. The most fundamental aspect of vector field topology is the extraction of first-order critical points. In the related dynamical systems literature (where phase spaces can be interpreted as vector fields), these points are referred to as fixed points, stationary points or singularities. The term *critical point* was coined for vector fields by Helman and Hesselink in their seminal work [HH89], which introduced vector field topology to the visualization community. Traditionally, the term critical point refers to a minimum, maximum or saddle in a scalar field. Throughout the visualization literature, however, the term critical point is also frequently used in the context of vector fields.

We follow Helman and Hesselink [HH89] and formally introduce a critical point $\mathbf{x}_c$ as a location at which the velocity vanishes:

$$\mathbf{v}(\mathbf{x}_c) = \mathbf{0}. \tag{27}$$

For their classification, we additionally require that the vector field is non-zero in the vicinity of the point $\mathbf{v}(\mathbf{x}_c + \varepsilon) \neq \mathbf{0}$, i.e., it is an *isolated* critical point. Further, for a first-order classification, we require that $\mathbf{v}$ is differentiable and that the Jacobian $\mathbf{J} = \nabla\mathbf{v}(\mathbf{x}_c)$ is non-singular. If this is fulfilled, the eigenvalues and eigenvectors of the Jacobian characterize the behavior of the flow around the critical point.

Under certain circumstances, selected types of critical points cannot exist. In divergence-free flows for instance, sources and sinks never occur. Higher-dimensional flows that describe the motion of finite-sized objects do not contain sources [GT16, GG17] and time-dependent flows do not contain any critical points in space-time, since particles always move forward in time, cf. Eq. (7).

Classification of Critical Points. Fig. 4 gives an overview of the types of isolated first-order critical points that may arise in 2D steady vector fields [HH89]. Each eigenvalue characterizes the behavior of the flow in the direction of the corresponding eigenvector. If both eigenvalues have positive real parts, the critical point is repelling. If both are negative, it is attracting. If the real parts of the two eigenvalues have opposite signs, a saddle is present. If the eigenvalues are complex, they indicate a swirling motion, which corresponds to vortical behavior. In this case, the critical point is called focus. A focus with zero real parts is called center. Critical points can likewise be studies in 3D, where the additional third eigenvector always has a real eigenvalue [HH91]. When extending topology beyond first-order, critical points may exhibit parabolic, hyperbolic and elliptic behavior in their vicinity [SKMR98].

Extraction of Critical Points. The extraction of first-order critical points boils down to a multi-variate root finding problem, i.e., we are searching for the intersection of zero-level isolines of the vector field components. In bi-/trilinear vectors fields, the search is relatively easy. First, candidate cells can be determined by checking the signs of the components at the quad vertices. If all signs of any component are all positive or all negative, then the cell cannot contain a critical point [GLL91]. Inside a bilinear candidate cell, the intersections can be found by solving two bilinear equations. Similarly in a simplex, the location can be solved for analytically based on barycentric interpolation or by subdivision [XXLL10]. Likewise, cells can be subdivided, either iteratively with nested intervals (2D/3D) or recursively into 4 quads (2D) or 8 volumes (3D) in case the sign check indicated that the cell contained critical points. This numerical procedure, however, tends to produce the same solutions multiple times, thus the result needs to be cleaned up in a post-process to remove duplicates. To reduce this problem, it is possible to subdivide until a certain minimal cell size is reached and to use multi-variate Newton iterations afterwards to converge to an accurate solution. Note that the multi-variate Newton method only finds one solution, thus the minimal cell size must be set small enough.

The paths of critical points can also be tracked by integration in space-time using feature flow fields [TS03]. The selection of seeds, however, is not trivial, as they might belong to curves that have already been traced. Further, numerical integration errors might accumulated, which however, can be addressed by stable feature flow fields [WTGP11] that use an additional force that pushes the numerically integrated curve back onto the critical line.

Working with first-order critical points places the inherent assumption that the flow is linear around critical points. Scheuermann et al. [SKMR98] extracted higher-order critical points in non-linear flows by using Clifford algebra. The search for higher-order critical points on non-planar surfaces received attention by Laramee et al. [LCJK*09] and by Li et al. [LVRL06] using polar coordinate representations. Tricoche et al. [TSH00] combined piecewise linear interpolation with a clustering of first-order critical points. Theisel [The02] designed piecewise linear planar vectors of arbitrary topology. For 2D flows, Effenberger and Weiskopf [EW10] proposed a cell-based approach that utilizes group theory.

Extensions of Critical Points and Further Reading. Helman and Hesselink extended the topological methods to 3D [HH91], including the classification of first-order critical points, separatrices starting at saddles and attachment/detachment points at no-slip boundaries. Further elements of the topological skeleton include boundary switch points [dLvL99], closed streamlines [WS01, TWHS04], saddle connectors [TWHS03] and boundary switch

connectors [WTHS04a]. The topology in two-parameter dependent vector fields was studied by Weinkauf et al. [WTHS06]. Further examples of vector field topology in 3D can be found in [GLL91, LDG98, MBS*04]. For further reading we refer to the reports of Heine et al. [HLH*16], Laramee et al. [LHZP07] and Pobitzer et al. [PPF*11], Scheuermann and Tricoche [ST05], and Weinkauf [Wei08].

2.4. Parallel Vectors Operator

As we will show later in Section 5.2, many vortex coreline definitions can be expressed as the union of points at which two vector fields are parallel. Peikert and Roth [PR99] introduced the *Parallel Vectors Operator* (PV), which returns the set of points at which two given vector fields $\mathbf{v}(\mathbf{x})$ and $\mathbf{w}(\mathbf{x})$ are parallel:

$$\mathbf{v}(\mathbf{x}) \parallel \mathbf{w}(\mathbf{x}) = \{\mathbf{x} : \mathbf{v}(\mathbf{x}) = \mathbf{0}\} \cup \{\mathbf{x} : \exists \lambda, \mathbf{w}(\mathbf{x}) = \lambda \mathbf{v}(\mathbf{x})\} \quad (28)$$

The solutions to this operator are curves that are either closed or connected with the boundary. It should be noted that PV curves can intersect. The PV operator can be used to define numerous features, including vortex corelines, separation lines, ridge lines and valley lines. Several methods have been proposed to extract PV curves, which can be categorized into local and integration-based methods.

Local Methods. Local methods subdivide the domain into cells (or operate on the cells on which the data set is given), solve for PV points on each cell boundary independently and connect the results afterwards in a post-process. Peikert and Roth [PR99] discussed several approaches to extract PV curves. In 3D, PV curves can be found as the intersection of zero-level isosurfaces of two components of the cross product: $\mathbf{v}(\mathbf{x}) \times \mathbf{w}(\mathbf{x})$. The third component must be checked for being zero as well. When the vector field is given on grids, the intersections of the PV curves with the grid faces can be found by Newton iterations. Further, for triangular faces they derived an analytic solution based on barycentric coordinates. Once the intersection points on the cell boundaries are found, line segments are formed within the cells and adjacent cells are connected. For cell-based extractions, Ju et al. [JCWD14] recently proposed a robust parity test to determine the number of PV points per cell face. When it comes to vortices, we are usually only interested in PV curves that exist in areas, where eigenvalues of the Jacobian are complex, i.e., areas in which swirling motion is present. To speed up the PV extraction, cells that only contain real-valued eigenvalues can be skipped.

Integration-based Methods. Local PV extraction as described above typically produces rather spurious results. There are a number of alternatives for closed PV line extraction including the curve-following predictor-corrector method of Peikert and Roth [PR99], the PVsolve algorithm of van Gelder and Pang [VGP09], the use of stable feature flow fields as in Weinkauf et al. [WTGP11], or the extractor of Pagot et al. [POS*11] for higher-order data.

PV Curve Filtering. Once PV curves are extracted, filtering is often required to clean up the result [WSTH07, GST16]. When using local methods, corelines are often spurious, i.e., several points might have been missed. To fill in gaps, lines can be merged if their end points are nearby and if the tangents at the end points are aligned. Often, lines are filtered by length by a user-defined threshold. When it comes to vortex corelines, curves are frequently rejected if the coreline tangent is not aligned with the flow, since ideally, vortex corelines should be pathlines, cf. Section 5.10 on vortex verification.

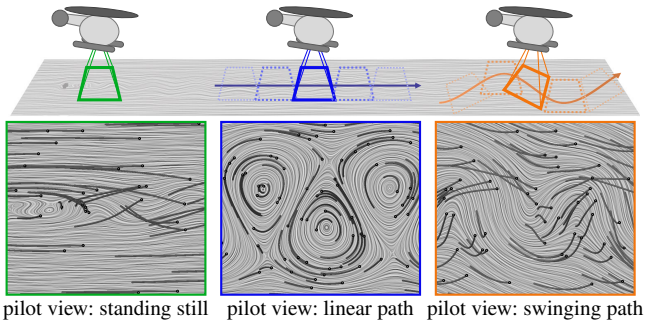

Figure 5: Most flow visualization techniques depend on the movement of the observer. Here, a line integral convolution (time slice) and pathlines (black) are shown for three different reference frame movements: standing still, linearly translating and swinging along a sine curve–unfortunately, all give different results. The illustration is courtesy from [GGT17].

3. Reference Frame Invariance

Vortex measures can be categorized by the types of reference frame motion under which the result of the vortex measure does not change. When we observe physical properties in the real world, for instance the temperature in a room, we want the measurement reading to be independent of the way how the measurement device moves. For scalar attributes, such as temperature, this is trivially fulfilled. When we observe vector- or tensor-valued properties, however, the observer's movement usually influences the result. This is also true for scalar measures that are derived from vector fields or tensor fields, such as velocity magnitude. An example for reference frame dependence is shown in Fig. 5, where a vector field is observed from the view of several pilots, moving in different ways over the domain. Each pilot sees the vector field differently.

The choice of an adequate reference frame is of highest importance for the successful characterization of a vortex [Lug79, Rob91]. Fig. 6 illustrates the two conceptually different approaches to vortex tracking in unsteady flows:

1. Some techniques estimate a suitable reference frame, e.g., by subtraction of some ambient flow, which is followed by an application of standard vortex extraction techniques in the resulting vector field, see Figs. 6b and 6c. Examples of such techniques follow in Sections 5.6 and 5.7.
2. Other techniques are invariant under certain types of reference frame motion, i.e., the result is the same, regardless of whether an ambient flow was subtracted or not, see Fig. 6d. The invariance of a measure under a certain type of reference frame motion directly translates to the ability to track vortices that perform this specific type of motion.

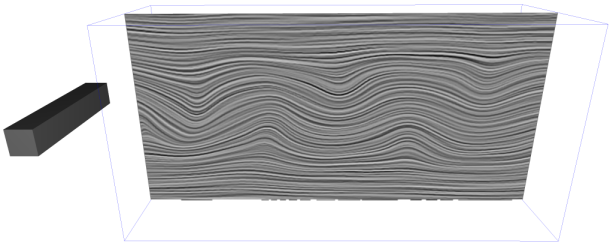

(a) Unsteady vector field $\mathbf{u}(\mathbf{x},t)$, shown using LIC (streamlines). Vortices are not apparent.

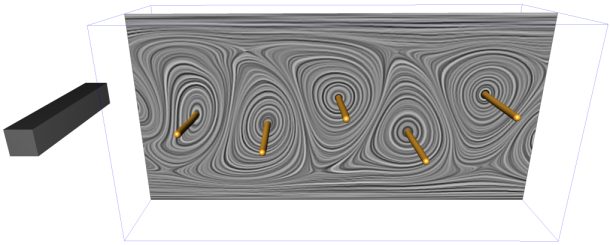

(b) Subtraction of the "right" ambient flow, reveals vortices, extracted with Sujudi-Haimes [SH95].

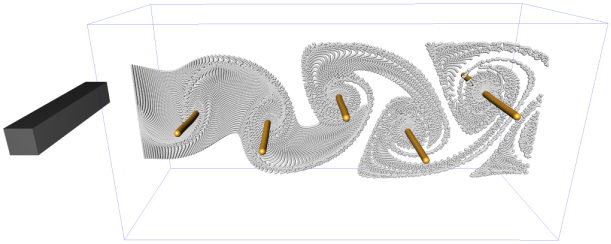

(c) Extracted vortex corelines in (b) are indeed centers of rotating particle motion.

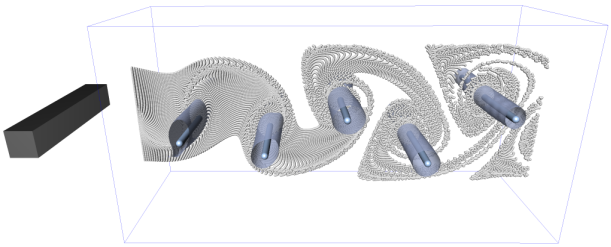

(d) *Galilean invariant* methods find vortices *without* subtraction of ambient flow. Here, λ_2 isosurfaces [JH95] and pathline corelines [WSTH07].

Figure 6: Overview of the two approaches to vortex tracking: subtracting a suitable ambient flow (b)–(c) or the invariance to certain types of vortex motion (d). Illustration from [Gün16].

In the following, we introduce the most important classes of reference frame invariance.

3.1. Galilean Invariance

Galilean invariance is the invariance of a measure under equal-speed translations of the reference frame of the form:

$$\mathbf{x}^* = \mathbf{x} + \mathbf{c}_0 + t\,\mathbf{c}_1 \quad , \quad t^* = t - a \tag{29}$$

where $\mathbf{c}_0$ and $\mathbf{c}_1$ are constant vectors. All measures that are derived from the spatial derivatives of the vector field, i.e., the Jacobian $\mathbf{J}$, are Galilean invariant. Among the derived quantities that include temporal derivatives, there are only few quantities that are Galilean invariant, namely acceleration $\mathbf{a}$ in Eq. (22) and the subtraction of the feature flow field $(\mathbf{v}-\mathbf{f})$. The proof of their Galilean invariance was privately communicated by Ronald Peikert and was acknowledged and documented by Sahner [Sah09]. Since $\mathbf{J}$ and $\mathbf{a}$ are Galilean invariant, the Galilean invariance of $(\mathbf{v}-\mathbf{f})$ also follows from the relation [Gün16]:

$$\mathbf{v} - \mathbf{f} = \mathbf{J}^{-1}\,\mathbf{a} \tag{30}$$

All Galilean invariant vortex extractors are able to track vortices that perform equal-speed translations. If a vortex performs any other type of movement, Galilean invariant methods will not produce the correct solution. Nevertheless, Galilean invariant methods are currently the most-spread approaches in practice.

3.2. Rotation Invariance

A vortex measure is *rotation invariant* if it is invariant under any equal speed rotation of the reference frame around a known center of rotation $\mathbf{x}_0$ [GST16]:

$$\mathbf{x}^* = \mathbf{Q}(t)(\mathbf{x}-\mathbf{x}_0) + \mathbf{x}_0 \quad , \quad t^* = t - a\,, \tag{31}$$

where $\mathbf{Q}(t)$ is an equal-speed rotation matrix and a is a constant. Rotation invariant methods are able to track vortices that perform equal-speed rotations. The main disadvantage of this formulation is that the rotation center $\mathbf{x}_0$ (and in 3D the rotation axis) must be known by the user in advance.

3.3. Objectivity

Current state-of-the-art feature extractors aspire to be *objective*, [Hal15, HHFH16, GGT17]. In continuum mechanics, objectivity refers to the invariance of a measure under a change of the reference frame that transforms a point $(\mathbf{x},t)$ in space-time to a new point $(\mathbf{x}^*,t^*)$ by

$$\mathbf{x}^* = \mathbf{Q}(t)\,\mathbf{x} + \mathbf{c}(t) \quad , \quad t^* = t - a \tag{32}$$

where $\mathbf{Q} \in SO(3)$ is a rotation matrix, $\mathbf{c}$ is a translation vector, and a is a constant. We assume $\mathbf{Q}$ and $\mathbf{c}$ to be smooth functions of t, cf. [TN65]. This means, objective measures are invariant under any smooth rotation and translation of the reference frame and thus, objective techniques are able to track vortices that perform any smooth rotation and translation in the domain. The definition of objectivity can be formalized [TN65]:

Definition 1 A scalar s is objective if it remains unchanged under any change of the reference frame as in Eq. (32). A vector $\mathbf{r}$ is objective if Eq. (32) transforms it to $\mathbf{r}^* = \mathbf{Q}(t)\,\mathbf{r}$. A second-order tensor $\mathbf{T}$ is objective if Eq. (32) transforms it to $\mathbf{T}^* = \mathbf{Q}(t)\,\mathbf{T}\,\mathbf{Q}(t)^{\mathrm{T}}$.

Generally, $\mathbf{v}$, $\mathbf{v}_t$, $\mathbf{J}$, $\mathbf{a}$ and $\boldsymbol{\Omega}$ are not objective, as they do not fulfill Definition 1, cf. [GGT17]. The divergence $\nabla\cdot\mathbf{v}$ and the strain rate tensor $\mathbf{S}$ are some of the few objective first-order differential properties of a vector field, which may be used to characterize a vortex in an objective way, cf. [Hal05, GGT17]. The objectivity of divergence is easily seen, since it can be computed from $\mathbf{S}$ as $\nabla\cdot\mathbf{v} = tr(\mathbf{S})$. It should be noted that every measure that is only

	Region-based	Line-based	Geometry-/integration-based	Vortex boundary
No invariance	helicity [Mof69] norm. helicity [LSD90] majority voting [BHD*15] Reynolds decomp. [Rey94] Helmholtz-Hodge [BNPB13] vector potential [TLHD03] combinatorial topo [JMT02b]	reduced velocity [SH95]^{3D} bent coreline [RP98] track CP [BP02, TSW*05] Fuchs et al. [FPH*08]	focus saddle line [GLL91]^{3D,L} skeleton growing [VV92] curvature center [SP99] winding angle [Por98, SP99] streamline sector [XXLL10] closed streaml. [WS01, TWHS04]	Rankine model [GTS*04] Max nested streaml. [Lag75]^{2D} Nested vortices [PKPH09]^{2D}
Galilean invariance	vorticity ω N_k [Tru53] λ_2-criterion [JH95] Δ-*criterion* [CPC90] Q-criterion [Hun87] Γ_2-*criterion* [GMG01]^{2D} Okubo-Weiss [Oku70, Wei91]^{2D} High-ord. OW [HK98, HMK98]^{2D} λ_{ci} [ZABK99] $\lambda_{cr}/\lambda_{ci}$ [CBA05] acceleration **a** [KRHH11]	reduced velocity [SH95]^{2D} Weinkauf et al. [WSTH07] vanishing **a** [KRHH11] λ_2 min [SWH05a, SVG*08] $det(\mathbf{J})$ extrema [BHJ16]^{2D}	predictor-corrector [BS95]^{P,L} vorticity line [MK85]^{L} rel. particle dist [CQB99]^{L}	ω / pressure thresh. [BS95]
Objectivity	pressure [HWM88, Rob90]^{P} Astarita [Ast79] rel. vorticity tens. [DL76, TK94] M_z-criterion [Hal05]^{3D,L} IVD [HHFH16] LAVD [HHFH16]^{L} near-steady frame [GGT17]	pressure minimum [MK97]^{P} vorticity maximum [SKA99] M_z extrema [SWTH07] near-steady frame [GGT17]	density estimate [WCW*09]^{L} streakline density [WT10]^{L}	elliptic LCS [Hal15]^{L} Eulerian variational [SH16b]
Other	rotation inv. [GST16]	rotation inv. [GST16]		

^{P}: pressure required, ^{L}: Lagrangian / integration-based, ^{2D}: only for 2D, ^{3D}: only for 3D

Table 1: Classification of vortex definitions. Techniques without an invariance work only for steady flows. Extremum lines of any region-based methods are by definition line-based and inherit the invariance of the region-based approach (the only exception is vorticity, which becomes objective). Lagrangian smoothing [FPS*08, STH*09] turns any Eulerian measure into a Lagrangian. Several more vortex measure can be derived by applying an existing technique in a certain reference frame [GGT17] or by replacing one of the building blocks of the vortex measure, such as the vorticity tensor by an objective counterpart [DL76, TK94, Hal05]. From any region-based method, vortex boundaries may be derived by thresholding. These additions are discussed in the remainder of the paper.

based on second-order spatial derivatives is also objective. Care should be taken, though. Not every objective measure automatically proves useful to be a good characterization of a vortex.

4. Classification of Vortex Extraction Techniques

Vortices are among the most important features in fluid flows and for this reason much research was devoted to their quantification, extraction and tracking. As there is no universal definition that captures all desired properties, a number of different vortex measures have been proposed in the literature. Table 1 gives an overview of the most important and most recent approaches. The rows distinguish between different degrees of reference frame invariance and the columns categorize the techniques into region-based, line-based and geometry-/integration-based methods, as well as boundary extraction methods.

The first row contains techniques that have no frame invariance, which means that these are techniques that are only applicable when either the flow is steady or when the flow is observed in the exact right reference frame in which it appears to be steady. The next two rows contain the two most important classes of reference frame invariance: Galilean invariance (from Section 3.1) and objectivity (from Section 3.3). The last row contains an additional class of reference frame invariance, i.e., rotation invariance.

The first column considers region-based methods, which identify regions of vortical behavior by deriving a scalar field that can be thresholded. Section 5.1 will explain these techniques in more detail. The second column lists line-based methods that seek for the coreline that particles are rotating around. These methods are detailed later in Section 5.2. The third column collects geometry-based (Section 5.3) and integration-based methods (Section 5.4), which derive vortex structures from the shape of streamlines or by observation of particles over time. The last column shows approaches that can be used to extract vortex boundaries (Section 5.8).

Table 1 identifies some additional properties that are relevant for the applicability: Superscripts tell whether a pressure field is required, numerical integration is necessary, or whether the methods

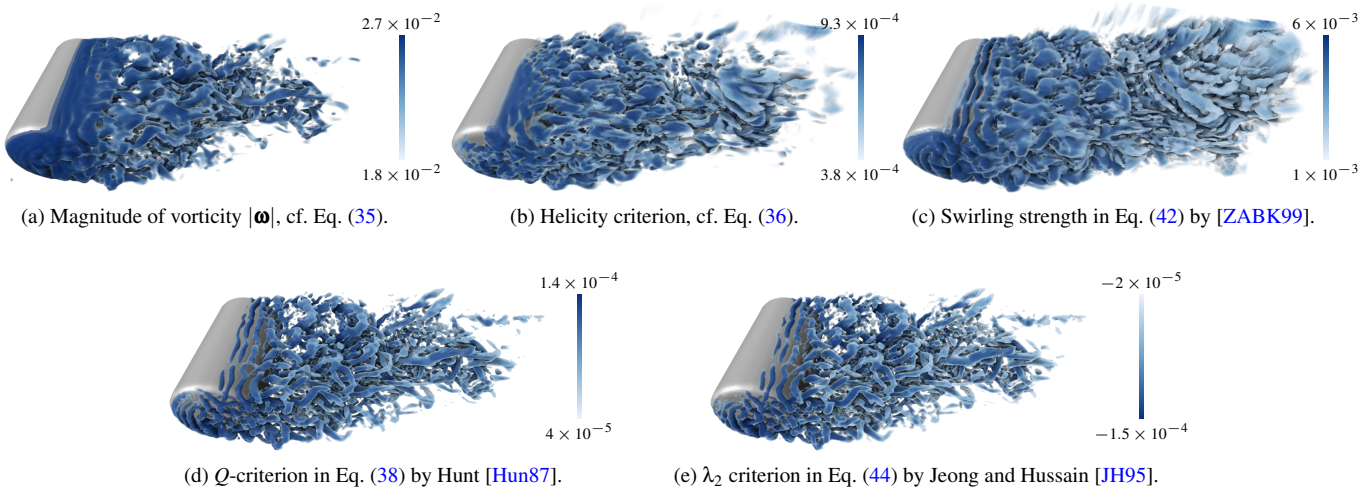

(a) Magnitude of vorticity $|\boldsymbol{\omega}|$, cf. Eq. (35).

(b) Helicity criterion, cf. Eq. (36).

(c) Swirling strength in Eq. (42) by [ZABK99].

(d) Q-criterion in Eq. (38) by Hunt [Hun87].

(e) λ_2 criterion in Eq. (44) by Jeong and Hussain [JH95].

Figure 7: Comparison of the most-common region-based methods in the turbulent flow behind a wall-mounted cylinder [FWT08]. Vorticity (a) produces false-positive near the obstacle. Helicity (b) is not Galilean invariant and does not produce nicely-connected vortex tubes. Swirling strength (c) conservatively shows too many regions, Q (d) and λ_2 (e) are known to give fairly similar results.

are applicable in 2D or 3D only. In the remainder of this paper, the techniques listed in Table 1 are explained in more detail.

5. Vortex Extraction Methods

The foundations of many formal vortex definitions were laid out between the late 70s and early 90s. For instance, Lugt [Lug79] defined vortices as follows:

> "Any mass of fluid moving around a common axis constitutes a vortex. Mathematically, such motion can be described by closed or spiraling streamlines (or pathlines) if a reference frame exists for which the flow field becomes steady."

Robinson [Rob91] proposed the following definition:

> "A vortex exists when instantaneous streamlines mapped onto a plane normal to the vortex core exhibit a roughly circular or spiral pattern, when viewed from a reference frame moving with the center of the vortex core."

Aside from being rather vague and not formal, both definitions include two subjects that are still actively researched to this day. Both require a definition of a *vortex coreline*, i.e., a line that particles rotate around, and they require that an *appropriate reference frame* is chosen, in which the velocity field becomes steady. The literature contains several other characterizations of a vortex, e.g., Blackwelder and Swearingen [BS90], and Portela [Por98].

In the following decades, these ideas were further formalized, which led to a wide range of vortex definitions. To this date, the problem of defining a general and precise vortex definition is not considered solved. In the following sections, we cover the existing work on region-based methods, vortex corelines and reference frames.

5.1. Region-based Methods

Region-based methods determine a volume of vortex-like behavior. In the following, we cover the most important approaches.

Pressure. In steady inviscid 2D flows, a pressure minimum can be found at the center of each rotating motion. Thus, a vortex can be identified as an area of low pressure by simple thresholding [HWM88]:

$$p \leq p_{thresh} \,, \tag{33}$$

which led to the search for elongated low-pressure regions in 3D [Rob90]. If the flow is unsteady, viscous or three-dimensional, a pressure minimum need not exist [CQB99].

Vorticity. The curl is also known as *vorticity* $\boldsymbol{\omega} = \nabla \times \mathbf{v}$, which is a Galilean-invariant quantity that can also be computed from the vorticity tensor $\boldsymbol{\Omega}$ in Eq. (14). Thereby, it can be defined in both 2D and 3D:

$$\text{2D: } \boldsymbol{\Omega} = \frac{1}{2}\begin{pmatrix} 0 & \omega \\ -\omega & 0 \end{pmatrix} \,, \quad \text{3D: } \boldsymbol{\Omega} = \frac{1}{2}\begin{pmatrix} 0 & -\omega_3 & \omega_2 \\ \omega_3 & 0 & -\omega_1 \\ -\omega_2 & \omega_1 & 0 \end{pmatrix} \tag{34}$$

In 2D, vorticity is a signed scalar ω, where the sign determines the rotation direction. In 3D, it is a vector-valued quantity $\boldsymbol{\omega} = (\omega_1, \omega_2, \omega_3)^{\mathrm{T}}$, and its magnitude $|\boldsymbol{\omega}|$ is twice the absolute angular velocity. Vorticity found numerous applications [KMM87, SPP04] and Fig. 7a gives an example. Simple thresholding, however,

$$|\boldsymbol{\omega}| \geq \omega_{thresh} \tag{35}$$

might produce false-positives in shear flow [Lug79, Rob91]. To address this problem, Sadlo et al. [SPP04] filtered vorticity isosurfaces based on the distance to boundaries or helicity. The latter is described next.

Helicity. To alleviate some of the shortcomings of vorticity, a threshold on *helicity* h [Mof69, Hus86] can be used instead:

$$h = (\nabla \times \mathbf{v}) \cdot \mathbf{v} \quad , \quad |h| \geq h_{thresh} \tag{36}$$

which excludes the shear flow false-positives, unless the shear layers are curved. Unlike vorticity, helicity is not Galilean-invariant [Hus86]. In fact, it heavily depends on the reference frame in which $\mathbf{v}$ is observed. Therefore, its usability in unsteady flows is limited. An example of helicity is shown in Fig. 7b. An extension is the *normalized helicity* h_n [LSD90], in which both velocity and vorticity are normalized before the dot product is computed.

$$h_n = \frac{\nabla \times \mathbf{v}}{|\nabla \times \mathbf{v}|} \cdot \frac{\mathbf{v}}{|\mathbf{v}|} \quad , \quad |h_n| \geq h_{thresh} \tag{37}$$

The advantage of this measure is that it is normalized to the range $[-1, 1]$. The sign indicates the swirling direction relative to the flow direction $\mathbf{v}$.

Q-criterion. In a three-dimensional divergence-free flow, the Galilean-invariant *Q-criterion* of Hunt [Hun87] considers a connected region to be a vortex if the second invariant of the Jacobian is positive. Using Eq. (18) with $\nabla \cdot \mathbf{v} = 0$ (divergence-free), the condition becomes:

$$\frac{1}{2}(\|\mathbf{\Omega}\|^2 - \|\mathbf{S}\|^2) > 0 \tag{38}$$

Eq. (38) shows that this criterion considers a vortex to be a region in which the Euclidean norm of the vorticity tensor $\mathbf{\Omega}$ is stronger than the Euclidean norm of the strain rate tensor $\mathbf{S}$. Fig. 7d gives an example. In addition, Hunt [Hun87] required that the pressure is lower inside the vortex than at its boundary. Note that $Q > 0$ does not guarantee a pressure minimum [JH95], but often the additional pressure condition is neglected [DD00, CBA05]. Truesdell [Tru53] defined the *kinematic vorticity number* $N_k = \frac{\|\mathbf{\Omega}\|}{\|\mathbf{S}\|}$. It should be noted that $N_k > 1 \Leftrightarrow Q > 0$ [JH95].

Okubo-Weiss criterion W. In a divergence-free 2D flow, the Jacobian $\mathbf{J}$ can be equivalently expressed as:

$$\mathbf{J} = \begin{pmatrix} \frac{\partial u}{\partial x} & \frac{\partial u}{\partial y} \\ \frac{\partial v}{\partial x} & \frac{\partial v}{\partial y} \end{pmatrix} = \frac{1}{2} \begin{pmatrix} s_1 & s_2 - w \\ s_2 + w & -s_1 \end{pmatrix} \tag{39}$$

with $s_1 = -2\frac{\partial v}{\partial y}$, $s_2 = \frac{\partial v}{\partial x} + \frac{\partial u}{\partial y}$ and $w = \frac{\partial v}{\partial x} - \frac{\partial u}{\partial y}$. Okubo [Oku70] and Weiss [Wei91] independently identified a vortex as a region with elliptic flow movement by the parameter:

$$W = u_y v_x + v_y^2 = \frac{1}{4}(s_1^2 + s_2^2 - w^2) = -det(\mathbf{J}) < 0 \tag{40}$$

Since $W = -det(\mathbf{J})$ and $Q = det(\mathbf{J})$ in 2D, cf. Eq. (21), the Okubo-Weiss criterion is considered as the 2D version of the Q-criterion. Hua and Klein [HK98], and Hua et al. [HMK98] proposed higher-order extensions of Okobu-Weiss by including acceleration terms.

Δ-criterion. Another Galilean-invariant criterion is the *Δ-criterion* of Chong et al. [CPC90]. This method determines when the characteristic equation of the Jacobian in Eq. (15) has complex solutions, see also Hunt et al. [HWM88]. Or in other words: it determines whether the Jacobian has complex eigenvalues. For a divergence-free flow, we have $P = 0$ in Eq. (15), and thus the discriminant of the characteristic equation is for 3D flows:

$$\Delta = \left(\frac{Q}{3}\right)^3 + \left(\frac{R}{2}\right)^2 > 0 \tag{41}$$

Generally, $\Delta > 0$ is less restricting than $Q > 0$, thus the Δ-criterion identifies larger vortex regions, cf. [CBA05].

Related to the Δ-criterion is the *swirling strength criterion*. Let $\lambda_{cr} \pm i\lambda_{ci}$ be the complex-conjugate eigenvalues of $\mathbf{J}$, Zhou et al. [ZABK99] characterized a vortex as region with sufficiently strong imaginary parts by

$$\lambda_{ci} > i_{thresh}. \tag{42}$$

This criterion is often too conservative, see Fig. 7c for an example. Chakraborty et al. [CBA05] extended this by additionally restricting the *inverse spiraling compactness* $\frac{\lambda_{cr}}{\lambda_{ci}} < c_{thresh}$, which favors streamline orbits.

λ_2-criterion. The pressure-minimum requirement fails under strong unsteady irrotational straining and viscous effects, thus Jeong and Hussain [JH95] neglected these effects. By taking the gradient of the reduced incompressible Navier-Stokes equation and by decomposing the Jacobian into symmetric and anti-symmetric parts they derived the reduced strain rate transport equation:

$$\mathbf{S}^2 + \mathbf{\Omega}^2 = -\frac{1}{\rho}\nabla(\nabla p) \, , \tag{43}$$

where $\nabla(\nabla p)$ is the Hessian matrix of the pressure. A pressure minimum inside a plane is present, if the Hessian has two positive eigenvalues. Let $\lambda_1 \geq \lambda_2 \geq \lambda_3$ be the eigenvalues of $\mathbf{S}^2 + \mathbf{\Omega}^2$, this is equivalent to requiring that the second largest eigenvalue λ_2 is negative, which is called the *λ_2-criterion*:

$$\lambda_2(\mathbf{S}^2 + \mathbf{\Omega}^2) < 0 \, . \tag{44}$$

Jeong and Hussain [JH95] noted that the eigenvalues of $\mathbf{S}^2 + \mathbf{\Omega}^2$ and Q are related by:

$$Q = -\frac{1}{2} tr(\mathbf{S}^2 + \mathbf{\Omega}^2) = -(\lambda_1 + \lambda_2 + \lambda_3) \tag{45}$$

They have shown that the Q criterion determines areas in which the vorticity tensor dominates the strain rate tensor over all directions, whereas λ_2 determines this excess only in a specific plane. Often, Q and λ_2 give fairly similar results, see Fig. 7e for an example. In fact, for incompressible 2D flows, Jeong and Hussain [JH95] have shown that $Q > 0$, $\lambda_2 < 0$ and $\Delta > 0$ give the same vortex region.

The λ_2 criterion neglects unsteady irrotational straining and viscous terms, and it is unclear how this affects the actual pressure distribution [CBA05]. Further, Cucitore [CQB99] emphasized that the pressure Hessian concept as defined above is not applicable for compressible flows. For more details on the relationships between these traditional vortex concepts, we refer to Chakraborty et al. [CBA05].

Γ_2-criterion For a 2D flow, Graftieaux et al. [GMG01] proposed the *Γ_2-criterion*. At each point $\mathbf{x}$, they defined a rectangular area S around it. They sampled area S with points $\mathbf{y}$ and define Γ_2 as:

$$\Gamma_2(\mathbf{x}) = \frac{1}{|S|} \int_{\mathbf{y} \in S} \sqrt{1 - \left(\frac{(\mathbf{v}(\mathbf{y}) - \mathbf{v}_{avg}(\mathbf{y}))^{\mathrm{T}} (\mathbf{y} - \mathbf{x})}{\|\mathbf{v}(\mathbf{y}) - \mathbf{v}_{avg}(\mathbf{y})\| \cdot \|\mathbf{y} - \mathbf{x}\|} \right)^2} \, \mathrm{d}S \tag{46}$$

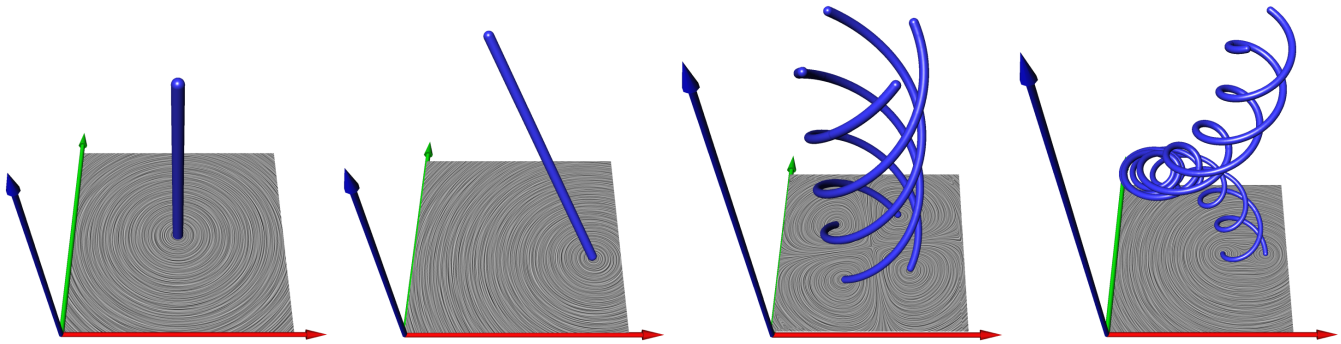

(a) In steady flows, vortex corelines are not moving. Standard critical point search is applicable, see Section 2.3.

(b) When vortices translate, Galilean invariance is required, Weinkauf et al. [WSTH07] in Eqs. (53) and (55).

(c) When vortices rotate, rotation invariance is necessary, Günther et al. [GST16] in Eqs. (62) and (63).

(d) When vortices rotate and translate, objectivity is required, Günther et al. [GGT17] in Eq. (95).

Figure 8: Overview of line-based methods that handle different types of vortex movements. In each example, a LIC slice depicts the vector field in the respective optimal reference frame, in which the flow appears steady. As can be seen, the streamlines rotate around the corelines.

Thereby, $\mathbf{v}_{avg}(\mathbf{y})$ is the average velocity in a stencil around $\mathbf{y}$, which is used to make the velocity relative to the neighborhood and thereby Galilean invariant. The selection of the size of both region S and the stencil radius for $\mathbf{v}_{avg}$ are both not trivial. This method determines whether the flow goes around point $\mathbf{x}$ by averaging the sine (with $\sin(x) = \sqrt{1-\cos(x)^2}$) of the angle between the (mean-free) flow direction at $\mathbf{y}$ and the direction toward the sampled point $\mathbf{y}$ inside region S. If $\mathbf{x}$ happens to be on the coreline of an axis-symmetric vortex (e.g., a perfect center), Γ_2 goes up toward 1.

Problems of Region-based Methods. Many of the vortex concepts above require a threshold to be set that is not necessarily constant along the vortex. Further note that all Q, Δ, λ_2 and Γ_2 are defined for divergence-free (incompressible) flows and that neither of them considers the unsteadiness of the flow [CBA05, Kol07].

Recent Developments. Biswas et al. [BHD*15] combined the four aforementioned local region-based vortex detectors via majority voting, namely Q, Δ, λ_2 and Γ_2. A region-based method finding nested vortices was developed by Petz et al. [PKPH09]. Kasten et al. [KRHH11] extracted Galilean invariant vortex regions by using the acceleration. Further, Kasten et al. [KHNH12] tracked vortex merging events over time by use of combinatorial scalar field topology. Combinatorial topology was also of concern in the vortex core region detection of Jiang et al. [JMT02b]. More region-based methods will follow in Section 5.5, which covers objective methods.

5.2. Line-based Methods

Line-based methods search for lines that particles rotate around.

Corelines in Steady Flow. In 2D steady flows, vortices can be found as critical points with complex eigenvalues, see Section 2.3. For steady flows in 3D, Globus et al. [GLL91] proposed to seed streamlines near focus saddle points in order to trace the vortex corelines. The streamlines are seeded a numerical epsilon away from the critical point in direction of the eigenvector that corresponds to the real-valued eigenvalue.

For a 3D steady flow $\mathbf{v}$, Sujudi and Haimes [SH95] defined the reduced velocity criterion, which considers the eigenvalues and eigenvectors of the Jacobian $\mathbf{J}$. A vortex coreline is present if two conditions are fulfilled. First, a pair of complex-conjugate eigenvalues exists, which is the necessary condition for swirling. Their two corresponding eigenvectors span the swirling plane, i.e., the plane in which the rotating motion occurs. Second, the eigenvector $\mathbf{e}$ to the remaining real eigenvalue fulfills:

$$\mathbf{v} - (\mathbf{v}^{\mathrm{T}}\mathbf{e})\mathbf{e} = \mathbf{0}\,. \tag{47}$$

That is, the projection of the flow vector $\mathbf{v}$ onto the swirling plane gives zero. This means that precisely on the coreline, the particles only move forward and are not rotating. This method extracts the coreline of swirling streamlines in 3D flow and has found many applications [KH97, GLT*07]. When applied in 2D space-time, this method is Galilean invariant. Peikert and Roth [PR99] formally defined the parallel vectors (PV) operator, which returns the set of points at which two vector fields are parallel. Using the PV operator, Sujudi-Haimes is equivalently expressed as:

$$\mathbf{v} \parallel \mathbf{J}\mathbf{v}, \tag{48}$$

i.e., $\mathbf{v}$ is parallel to an eigenvector of $\mathbf{J}$.

For steady flows, acceleration $\mathbf{a}$ can be expressed as $\mathbf{a} = \mathbf{J}\mathbf{v}$, cf. Eq. (22), and thus Eq. (48) is equivalent to $\mathbf{v} \parallel \mathbf{a}$. The curvature vector $\mathbf{c}$ of a streamline can be computed as [RP98]:

$$\mathbf{c} = \frac{\mathbf{v} \times \mathbf{a}}{\|\mathbf{v}\|^3} \tag{49}$$

If $\mathbf{v}$ and $\mathbf{a}$ are parallel, i.e., if we are on a vortex coreline, then Eq. (49) suggests that the streamline passing through this point is straight [PR99]. Thus, standard Sujudi-Haimes [SH95] favors straight corelines. Based on this observation, a higher-order method was described by Roth and Peikert [RP98] to extract bent vortex corelines. Using the parallel vectors operator, they proposed to find places where the derivative of the acceleration is parallel to the

flow:

$$\frac{D\mathbf{a}}{Dt} \parallel \mathbf{v} \tag{50}$$

In steady flows, this simplifies to $(\nabla \mathbf{a})\mathbf{v} \parallel \mathbf{v}$. Fuchs et al. [FPH*08] recommended to try traditional Sujudi-Haimes first and experiment with the higher-order method only if Sujudi-Haimes does not produce the desired results, since the higher-order method amplifies numerical difficulties and involves a higher computation cost.

Another topological structure are bifurcation lines, which can be found with Eqs. (48) and (50), with the requirement that all eigenvalues are real-valued [PC87, Rot00, MSE13, MBES16].

Corelines in Unsteady Flow. For unsteady data, Bauer and Peikert [BP02], Tricoche et al. [TWSH02] and Theisel et al. [TSW*05] tracked the corelines of swirling streamlines over time. This makes sense for vortex tracking in instantaneous vector fields, such as in magnetic fields or when the vector field is transformed into a reference frame, in which the flow appears steady.

However, Weinkauf et al. [WSTH07] and Fuchs et al. [FPH*08] pointed out that the temporal derivative needs to be taken into account when studying particle motion in unsteady flows. In fact, Weinkauf et al. [WSTH07] and Fuchs et al. [FPH*08] found that pathlines swirl around a different coreline than streamlines and thus extended the method of Sujudi and Haimes in different ways to find corelines of swirling pathlines, i.e., the corelines of particles in unsteady flow. Weinkauf et al. [WSTH07] observed the four eigenvectors of the 4D space-time Jacobian $\bar{\mathbf{J}}$:

$$\underbrace{\begin{pmatrix}\mathbf{e}_1\\0\end{pmatrix}}_{\text{real}}, \underbrace{\begin{pmatrix}\mathbf{e}_2\\0\end{pmatrix}, \begin{pmatrix}\mathbf{e}_3\\0\end{pmatrix}}_{\text{complex}}, \underbrace{\begin{pmatrix}\mathbf{f}\\1\end{pmatrix}}_{\text{real}\,(0)} \tag{51}$$

Below the vectors, we denote whether the corresponding eigenvalues are real-valued or complex. W.l.o.g., we assume the vector containing $\mathbf{e}_1$ to be the eigenvector with real eigenvalue. Recalling from Section 2.2, we remind that one of the eigenvectors contains the feature flow field $\mathbf{f}$ from Eq. (26) and that the corresponding eigenvalue is 0. Following the idea of Sujudi and Haimes [SH95], Weinkauf et al. [WSTH07] searched for space-time locations at which the flow is in the plane that is spanned by the two eigenvectors that correspond to the two real eigenvalues, i.e., the flow is in the non-swirling subspace of the space-time domain. For $n = 3$, this leads to the following equivalent conditions for a non-singular Jacobian [WSTH07]:

$$\begin{pmatrix}\mathbf{v}\\1\end{pmatrix}, \begin{pmatrix}\mathbf{e}_1\\0\end{pmatrix}, \begin{pmatrix}\mathbf{f}\\1\end{pmatrix} \text{ are coplanar} \quad \Leftrightarrow \quad \mathbf{v}-\mathbf{f} \parallel \mathbf{e}_1 \tag{52}$$

$$\Leftrightarrow \quad \mathbf{v}-\mathbf{f} \parallel \mathbf{J}(\mathbf{v}-\mathbf{f}) \tag{53}$$

In Eq. (53) one might be tempted to ask, whether $\mathbf{J}$ should be computed from $\mathbf{v}$ or $(\mathbf{v}-\mathbf{f})$. If and only if the assumption of Galilean invariance is valid, i.e., if vortices perform equal-speed translations, then:

$$\mathbf{v}-\mathbf{f} \parallel \nabla(\mathbf{v}-\mathbf{f})(\mathbf{v}-\mathbf{f}) \quad \Leftrightarrow \quad \mathbf{v}-\mathbf{f} \parallel \nabla(\mathbf{v})(\mathbf{v}-\mathbf{f}). \tag{54}$$

since $\nabla \mathbf{f} = \mathbf{0}$. The two approaches differ only when $\nabla \mathbf{f} \neq \mathbf{0}$, which is relevant in different coordinate systems, e.g., in polar coordinates [GST16], or when vortices do not move with equal speed in a constant direction.

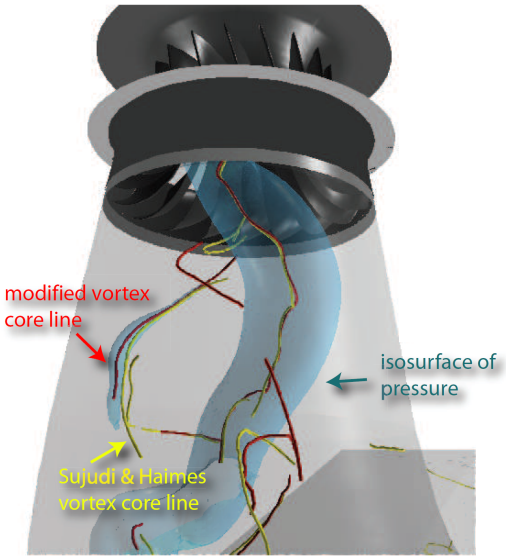

Figure 9: Comparison of vortex corelines that were extracted using the method of Fuchs et al. [FPH*08] in Eq. (56) with corelines extracted using Sujudi-Haimes [SH95] in Eq. (48). With the method of Fuchs et al. [FPH*08], the vortex coreline stays better inside the pressure isosurface, indicating that the extracted coreline is closer to the pressure minimum. This illustration is from [FPH*08].

For $n = 2$, we have the following Galilean invariant conditions that are all equivalent in areas of non-vanishing Jacobian:

$$\mathbf{a} = \mathbf{0} \quad \Leftrightarrow \quad \mathbf{v}-\mathbf{f} = \mathbf{0} \quad \Leftrightarrow \quad \bar{\mathbf{f}} \parallel \bar{\mathbf{p}} \quad \Leftrightarrow \quad \bar{\mathbf{J}}\,\bar{\mathbf{p}} \parallel \bar{\mathbf{p}}. \tag{55}$$

The equivalence of the four expressions in Eq. (55) follows directly from Eq. (30), $\bar{\mathbf{J}}\,\bar{\mathbf{p}} = \begin{pmatrix}\mathbf{a}\\0\end{pmatrix}$ and $\bar{\mathbf{p}} = \begin{pmatrix}\mathbf{v}\\1\end{pmatrix}$. As a side note, it means that for $n = 2$ the corelines of swirling particle motion [WSTH07] and vortices by vanishing acceleration [KRHH11, KHNH11] are identical. Fig. 8b shows a 2D vortex that is moving with equal speed in a constant direction, which was extracted using Eq. (55).

Fuchs et al. [FPH*08] based their extension of Sujudi-Haimes to the unsteady case on the acceleration. In the steady case, Sujudi-Haimes can be interpreted as $\mathbf{v} \parallel \mathbf{a}$. The acceleration of an unsteady flow is $\mathbf{a} = \mathbf{J}\mathbf{v} + \mathbf{v}_t$, cf. Eq. (22). In order to include the temporal derivative in unsteady flows, Fuchs et al. [FPH*08] used the unsteady acceleration in the parallel vectors condition: $\mathbf{v} \parallel \mathbf{J}\mathbf{v} + \mathbf{v}_t$. Since $\mathbf{J}(\mathbf{v}-\mathbf{f}) = \mathbf{a}$ from Eq. (30), their method is equivalently expressed by:

$$\mathbf{v} \parallel \mathbf{a} \quad \Leftrightarrow \quad \mathbf{v} \parallel \mathbf{J}\mathbf{v}+\mathbf{v}_t \quad \Leftrightarrow \quad \mathbf{v} \parallel \mathbf{J}(\mathbf{v}-\mathbf{f})\,. \tag{56}$$

Note that these conditions are not Galilean invariant. The last condition differs only by the subtraction of $\mathbf{f}$ on the left side from Weinkauf et al. [WSTH07] in Eq. (53).

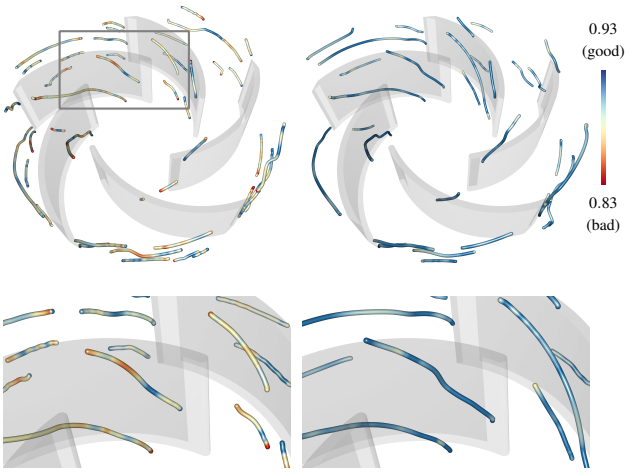

(a) Galilean invariant [WSTH07] (b) Rotation invariant [GST16]

Figure 10: Vortex corelines in a centrifugal pump that is viewed in a rotating reference frame in space-time. Galilean invariant vortex corelines (a) have a poorer tangent alignment than the rotation invariant corelines (b). The tangent alignment is color-coded and measures the angle between coreline tangent and the flow, see Eq. (100). The illustrations were provided by [GST16].

Rotation Invariant Vortices. Galilean invariant methods (both region-based and line-based) can be turned into rotation invariant methods by observing the flow in polar coordinates instead of Cartesian coordinates, since a rotation in Cartesian coordinates equals a translation in polar coordinates [GST16]. The transformation into polar coordinates can be performed analytically by a non-isometric domain deformation, which eventually leads to a replacement of Jacobian $\mathbf{J}$ by its rotation invariant counterpart $\mathbf{J}_r$ in the standard vortex measures. The rotation invariant Jacobian $\mathbf{J}_r$ has a simple closed-form [GST16]:

$$\mathbf{J}_r = \mathbf{J} + \frac{1}{d}\,\mathbf{R}\,\mathbf{H}\,\mathbf{R}^{\mathrm{T}} \tag{57}$$

In 2D, the matrices $\mathbf{R}$ and $\mathbf{H}$ are computed as:

$$d = \|\mathbf{x}-\mathbf{x}_0\| \quad , \quad \mathbf{r} = \frac{\mathbf{x}-\mathbf{x}_0}{d} \quad , \quad \mathbf{r}_p = \begin{pmatrix} 0 & 1 \\ -1 & 0 \end{pmatrix} \mathbf{r} \tag{58}$$

$$\mathbf{R} = (\mathbf{r}_p, \mathbf{r}) \quad , \quad \mathbf{H} = \begin{pmatrix} -\mathbf{u}^{\mathrm{T}}\mathbf{r} & -\mathbf{u}^{\mathrm{T}}\mathbf{r}_p \\ \mathbf{u}^{\mathrm{T}}\mathbf{r}_p & 0 \end{pmatrix} \tag{59}$$

In 3D, a normalized rotation axis $\mathbf{n}$ needs to be specified as well. Let $\mathbf{b}$ be the point on the rotation axis with shortest distance to $\mathbf{x}$, i.e., $(\mathbf{x}-\mathbf{b})^{\mathrm{T}}\mathbf{n} = 0$. Then, $\mathbf{R}$ and $\mathbf{H}$ can be computed using:

$$d = \|\mathbf{x}-\mathbf{b}\| \quad , \quad \mathbf{r} = \frac{\mathbf{x}-\mathbf{b}}{d} \quad , \quad \mathbf{r}_p = \mathbf{r}\times\mathbf{n} \tag{60}$$

$$\mathbf{R} = (\mathbf{r}_p, \mathbf{r}, \mathbf{n}) \quad , \quad \mathbf{H} = \begin{pmatrix} -\mathbf{u}^{\mathrm{T}}\mathbf{r} & -\mathbf{u}^{\mathrm{T}}\mathbf{r}_p & 0 \\ \mathbf{u}^{\mathrm{T}}\mathbf{r}_p & 0 & 0 \\ 0 & 0 & 0 \end{pmatrix}. \tag{61}$$

The main disadvantage of this method is that it requires the rotation center (and the axis in 3D) to be known by the user.

Using $\mathbf{a}_r = \mathbf{J}_r\,\mathbf{v} + \mathbf{v}_t$ and $\mathbf{f}_r = -\mathbf{J}_r^{-1}\,\mathbf{v}_t$, Günther et al. [GST16] defined rotation invariant vortex measures by replacing the Galilean invariant differential properties with their rotation invariant counterparts. For $n = 2$, they proposed the equivalent conditions:

$$\mathbf{a}_r = \mathbf{0} \quad \Leftrightarrow \quad \mathbf{v}-\mathbf{f}_r = \mathbf{0} \quad \Leftrightarrow \quad \bar{\mathbf{f}}_r \parallel \bar{\mathbf{p}} \quad \Leftrightarrow \quad \bar{\mathbf{J}}_r\,\bar{\mathbf{p}} \parallel \bar{\mathbf{p}}. \tag{62}$$

An example of a vortex that moves on a rotating path is shown in Fig. 8c. In Fig. 10, rotation invariant and Galilean invariant corelines are compared in the numerical simulation of a centrifugal pump. For $n = 3$, Günther et al. [GST16] proposed

$$\nabla(\mathbf{v}-\mathbf{f}_r)\cdot(\mathbf{v}-\mathbf{f}_r) \parallel (\mathbf{v}-\mathbf{f}_r) \tag{63}$$

For the definition of rotation invariant region-based measures, the rotation invariant Jacobian is decomposed into

$$\mathbf{J}_r = \mathbf{S}_r + \Omega_r \tag{64}$$

with the strain rate tensor $\mathbf{S}_r = \frac{1}{2}(\mathbf{J}_r + \mathbf{J}_r^{\mathrm{T}})$ and the vorticity tensor $\Omega_r = \frac{1}{2}(\mathbf{J}_r - \mathbf{J}_r^{\mathrm{T}})$. Following [JH95] in Eq. (44), they defined the rotation invariant λ_{2_r} criterion by considering the second-largest eigenvalue of $\mathbf{S}_r^2 + \Omega_r^2$:

$$\lambda_{2_r} = \lambda_2(\mathbf{S}_r^2 + \Omega_r^2) < 0. \tag{65}$$

Similarly, they followed [Hun87] in Eq. (38) and defined the rotation invariant Q_r criterion

$$Q_r = \frac{1}{2}\left(\|\Omega_r\|^2 - \|\mathbf{S}_r\|^2\right) > 0, \tag{66}$$

which characterizes vortices as regions in which the Euclidean norm of the rotation invariant vorticity tensor dominates that of the rotation invariant strain rate tensor.

Section 5.7 contains several additional line-based methods that are objective, i.e., they include Galilean invariant and rotation-invariant measures as a special case.

Extremum Lines. Line structures can also be extracted as extremal lines of region-based methods. For instance, Miura and Kida [MK97] identified vortex corelines as sectional extremum lines of pressure. Strawn et al. [SKA99] searched for lines on which the vorticity magnitude is maximized, cf. Eq. (34). As explained later in Section 5.5, the location of vorticity extrema is objective. Peikert and Roth [PR99] have shown that extremal lines in the normalized helicity field from Eq. (37) are locations where:

$$\mathbf{v} \parallel \nabla\times\mathbf{v}\,, \tag{67}$$

which are locations where the normalized helicity is $+1$ or -1. Sahner et al. [SWH05a] extracted extremum lines of both the λ_2-criterion and the Q-criterion by the use of feature flow fields [TS03]. Later, Sahner et al. [SWTH07] computed vortex and strain skeletons as extremal structures of the Q-criterion [Hun87] and the M_z-criterion [Hal05]. Fig. 11 gives an example of such a vortex and strain skeleton based on the Q-criterion. Schafhitzel et al. [SVG*08] further focused on the topology of λ_2-based vortex corelines.

Problems of Line-based Methods. As a result of their studies in aircraft aerodynamics, Kenwright and Haimes [KH97] formulated several problems that line-based vortex methods have to

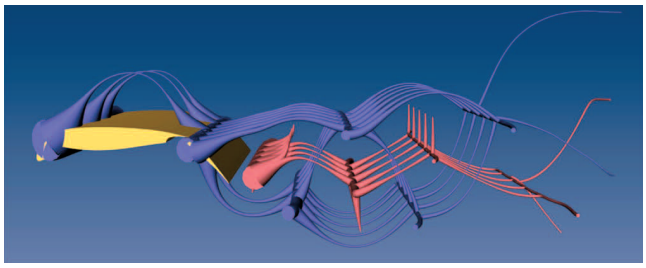

Figure 11: Visualization of the vortex and strain skeletons of Sahner et al. [SWTH07] based on the Q-criterion, showing lines of maximal strain (blue) and lines of maximal vortex activity (red). This illustration is from [SWTH07].

this day. Local coreline extractors often fail to produce contiguous lines. Integration-based methods exist, see Section 2.4, though they require careful placement of seed points, removal of duplicates and often require an additional error minimization to remove the otherwise accumulating integration errors. Further, coreline-based methods tend to contain false-positives, e.g., swirling can be found in boundary layers. Kenwright and Haimes [KH97], and Van Gelder [VG12] made aware that inaccurate results with local methods are not only attributed to (possible) lack of Galilean invariance, but also arise when swirling occurs at different scales. Thus, if the aerodynamics at a specific location is a sum of several effects (vortices at different scales [VG12] or a general bending of the coreline [RP96]), local methods will depend on the strongest effect and the extracted coreline will be displaced to some degree.

5.3. Geometric Methods

Villasenor and Vincent [VV92] tracked elongated vortex tubes in space and time by iteratively constructing a skeleton (the center line). Given a seed point of the skeleton (manually chosen or the location of a vorticity maximum), they probed about 100 candidate directions on a sphere with small cylinders. Within each cylinder, a score value was computed (e.g., average vorticity) and the skeleton was advanced in direction of the strongest score, which iteratively generated the center line of a vortex tube. To track the vortex tube over time, they assumed that the tube moved orthogonal to its tangent. In the tangent plane, they followed Archimedes' spiral outward to probe the neighborhood for high vorticity.

For 2D flows, Sadarjoen and Post [SP99,SP00] presented two geometric approaches that are based on the geometry of streamlines. Their *curvature center method* computes the density of curvature centers for a given set of streamlines. Assuming that many streamlines enclose the vortex core, the curvature centers are expected to occur most frequently near the center of a vortex core. The method works best for circular vortices, and the curvature center density is typically thresholded.

The *winding angle method* of Sadarjoen and Post [SP99] is inspired by Portela [Por98]. Their method first accumulates along each streamline the winding angle, i.e., the angle between two subsequent polyline segments. If a streamline performs a full loop, the winding angle is 2π. Sadarjoen and Post [SP99] only considered

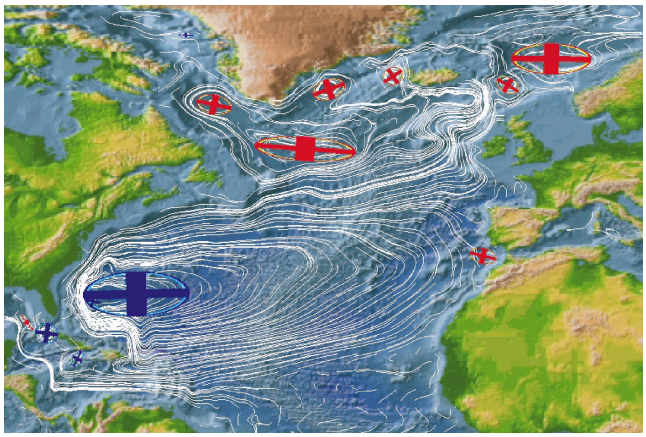

Figure 12: Streamlines and vortices in the Atlantic Ocean. Vortices are visualized by ellipses (the rotation direction is color-coded). This illustration is from [SP00].

streamlines for which the winding angle was above a threshold and the distance between seed point and end point of the streamline was below a certain threshold. The resulting set of streamlines was spatially clustered and ellipsis were fitted to each cluster to provide a visual representation. See Fig. 12 for an example of vortices in the Atlantic Ocean.

Given a set of candidate vortex cores in 2D, Xie et al. [XXLL10] moved the origin of the coordinate system to the center of the vortex and seeded a streamline near it. If the streamline intersects with the x-axis and y-axis on both the positive and negative side, then the streamline performed a full turn. Streamlines can then be filtered by the number of turns and the distance to the center of the vortex. This approach does not require estimation of derivatives. Actual closed streamlines can be found using the Poincaré theorem [WS01] or as the intersection of forward and backward integrated stream surfaces in space-time [TWHS04].

5.4. Integration-based Measures

Aside from the geometric methods, all aforementioned automatic extraction approaches have in common that they are local, and thus easily parallelized. However, it was shown that there are classes of vortices that cannot be extracted by local methods, for instance attracting vortices that move on non-linear paths. Thus, instead, integration-based methods were developed, such as the particle density estimation by Wiebel et al. [WCW*09]. They proposed to inject a number of particles and observe their attraction behavior over time. Weinkauf and Theisel [WT10] found attractors by analyzing the Jacobian of a derived vector field in which streaklines are tangent curves, see Fig. 13. Globus et al. [GLL91] seeded streamlines near focus saddle points in order to trace the vortex corelines in steady 3D flows, as previously detailed in Section 5.2. Banks and Singer [BS95] suggested a curve following vorticity-predictor, pressure-corrector method. Their method alternates between an integration step in the vorticity field $\boldsymbol{\omega}$ and a gradient descent toward the pressure minimum. For this, Peikert and Roth [PR99] defined a

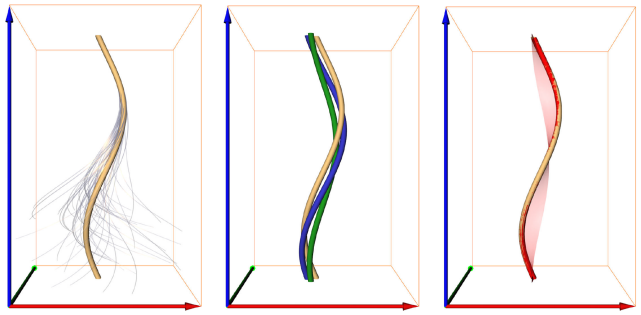

(a) Pathlines approach the attracting coreline (yellow).

(b) Stream (green) and pathline corelines (blue) do not match the attractor.

(c) Streakline corelines (red curve and surface) match the attractor.

Figure 13: The corelines of swirling streak lines (red) detect an attracting vortex (yellow) that moves on a rotating path. Streamline corelines (green, no invariance) and pathline corelines (blue, Galilean invariance) are not invariant under rotations of the observer. The streakline coreline sweeps in 4D over a surface shown in (c) together with its intersection at the respective time, which is a line in space-time that matches the attractor of this flow. The illustration is provided by [WT10].

parallel vectors formulation:

$$\nabla \times \mathbf{v} \parallel \nabla p, \tag{68}$$

which is local and thus yields spurious solutions with potential false-positives.

Moin and Kim [MK85] traced streamlines in the normalized vorticity field, which they called vortex lines $\mathbf{x}(s)$:

$$\frac{\mathrm{d}\mathbf{x}(s)}{\mathrm{d}s} = \frac{\boldsymbol{\omega}}{|\boldsymbol{\omega}|} \tag{69}$$

Similarly, such vortex lines (or vorticity field lines) have been placed by Sadlo et al. [SPP04], who adapted the density of the lines to the vorticity magnitude. As shown by Robinson [Rob91], vortex lines are difficult to seed and can be misleading even when seeded close to an actual vortex. Another Lagrangian detector was developed by Cucitore et al. [CQB99]. They observed the evolution of the relative distance between two nearby-released particles compared to the similarity of their particle trajectories. Inside a vortex, the relative distance is assumed to remain small. Since their method may also respond to non-vortical flows, they propose to additionally apply the Δ-criterion of Chong et al. [CPC90], i.e., to check for the presence of complex eigenvalues.

Further, Lagrangian smoothing as proposed by Fuchs et al. [FPS*08] and Shi et al. [STH*09] can be applied to any local vortex detector, which smoothes the extraction results along pathlines over time.

5.5. Objective Methods

The following section is entirely devoted to objective techniques.

Relative Vorticity Tensor-based Measures. While strain rate tensor $\mathbf{S}$ is objective, vorticity tensor $\boldsymbol{\Omega}$ is only Galilean invariant. To obtain an objective vorticity tensor, Drouot and Lucius [DL76] built the *relative vorticity tensor* $\breve{\boldsymbol{\Omega}}$, which views vorticity in strain basis:

$$\breve{\boldsymbol{\Omega}} = \boldsymbol{\Omega} - \mathbf{W} \tag{70}$$

Thereby, the rate-of-rotation tensor $\mathbf{W}$ is given by: $\mathrm{D}\mathbf{e}_i/\mathrm{D}t = \mathbf{W}\mathbf{e}_i$, with $\mathbf{e}_i$ being the unit eigenvectors of $\mathbf{S}$ and $\mathrm{D}/\mathrm{D}t$ being the material derivative. The tensor $\breve{\boldsymbol{\Omega}}$ was independently identified by Dresselhaus and Tabor [DT92], and Tabor and Klapper [TK94], who called it *effective rotation*. Astarita [Ast79] proved the objectivity of Eq. (70) and proposed an index that classifies the domain into extension-like motions and rigid-body-like rotations. When substituting the vorticity tensor $\boldsymbol{\Omega}$ by the relative vorticity tensor $\breve{\boldsymbol{\Omega}}$, traditional region-based methods can be made objective. An objective counterpart to the Q criterion is, cf. Haller [Hal05]:

$$\frac{\|\breve{\boldsymbol{\Omega}}\|^2 - \|\mathbf{S}\|^2}{2} > 0 \tag{71}$$

An objective counterpart to λ_2 is, cf. Martins et al. [MPM*16]:

$$\lambda_2(\mathbf{S}^2 + \breve{\boldsymbol{\Omega}}^2) < 0 \tag{72}$$

which is illustrated in Fig. 14a. Martins et al. [MPM*16] also defined objective counterparts to the Δ-criterion [CPC90] and the inverse spiraling compactness [CBA05]. We refer to Thompson [Tho08] for a fluid mechanics perspective on recent advances in this area.

Strain Tensor-based Measures. Haller [Hal05] proposed the M_z criterion, which defines a vortex as a set of fluid trajectories in an incompressible flow along which the strain acceleration tensor $\mathbf{M}$:

$$\mathbf{M} = \mathbf{S}\mathbf{J} + \mathbf{J}^{\mathrm{T}}\mathbf{S} + \frac{\mathrm{d}}{\mathrm{d}t}\mathbf{S}(\mathbf{x}(t),t) \tag{73}$$

$$= \mathbf{S}\mathbf{J} + \mathbf{J}^{\mathrm{T}}\mathbf{S} + \mathbf{S}_x u + \mathbf{S}_y v + \mathbf{S}_z w + \mathbf{S}_t \tag{74}$$

is indefinite over directions of zero strain. Here, $\mathbf{v} = (u,v,w)^{\mathrm{T}}$, $\mathbf{J} = \nabla\mathbf{v}$, $\mathbf{S}$ is the strain rate tensor, cf. Eq. (14), and $\mathbf{S}_x = \frac{\mathrm{d}\mathbf{S}}{\mathrm{d}x}$, $\mathbf{S}_y = \frac{\mathrm{d}\mathbf{S}}{\mathrm{d}y}$, $\mathbf{S}_z = \frac{\mathrm{d}\mathbf{S}}{\mathrm{d}z}$ and $\mathbf{S}_t = \frac{\mathrm{d}\mathbf{S}}{\mathrm{d}t}$ are the partial derivatives of $\mathbf{S}$. Haller [Hal05] computed a binary field that indicates whether the tensor is indefinite, which in turn marks non-hyperbolic particle behavior. For this, $\mathbf{M}$ is considered in strain basis. Let $\mathbf{e}_1, \mathbf{e}_2, \mathbf{e}_3$ be the eigenvectors of $\mathbf{S}$ with corresponding eigenvalues $\lambda_1, \lambda_2, \lambda_3$ such that $sign(\lambda_1) = sign(\lambda_2) \neq sign(\lambda_3)$ and $|\lambda_1| \geq |\lambda_2|$. Then, $\mathbf{M}$ is in strain basis:

$$\widehat{\mathbf{M}} = (\mathbf{e}_1, \mathbf{e}_2, \mathbf{e}_3)^{\mathrm{T}}\mathbf{M}\,(\mathbf{e}_1, \mathbf{e}_2, \mathbf{e}_3) \tag{75}$$

Haller [Hal05] proposed two approaches to determine whether tensor $\mathbf{M}$ is indefinite. One may either check whether the function

$$m(\alpha) = \widehat{\mathbf{M}}_{11} b\cos^2\alpha + \widehat{\mathbf{M}}_{22} a\sin^2\alpha + \widehat{\mathbf{M}}_{33} ab \tag{76}$$

$$+ \sqrt{ab}\left(2\widehat{\mathbf{M}}_{13}\sqrt{b}\cos\alpha + 2\widehat{\mathbf{M}}_{23}\sqrt{a}\sin\alpha + \widehat{\mathbf{M}}_{12}\sin 2\alpha\right) \tag{77}$$

with $a = -\frac{\lambda_1}{\lambda_3}$ and $b = 1 - a$, is everywhere positive in the range $\alpha \in [0, 2\pi]$. For this, $m(\alpha)$ is sufficiently densely sampled. Sahner et al. [SWTH07] demonstrated that the search can be accelerated by a factor of three when a bisection approach is combined with a first-order derivative estimation. Alternatively, Haller [Hal05] defined

(a) The λ_2 criterion based on the relative vorticity tensor, cf. Eq. (72).

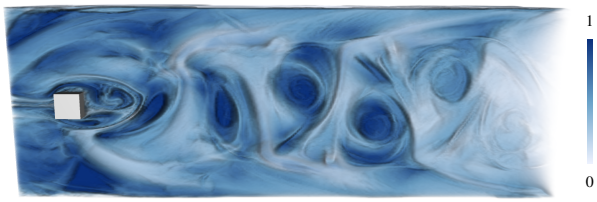

(b) The M_z criterion in Eq. (78) of Haller [Hal05].

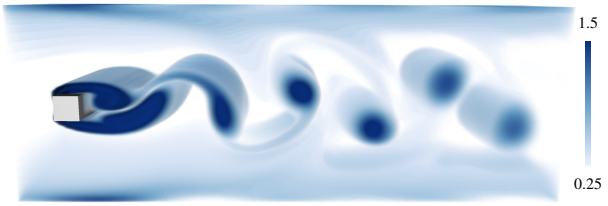

(c) IVD in Eq. (80) by Haller et al. [HHFH16].

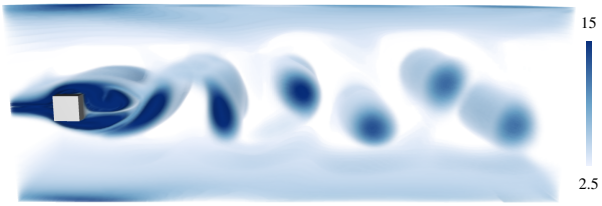

(d) LAVD in Eq. (81) by Haller et al. [HHFH16].

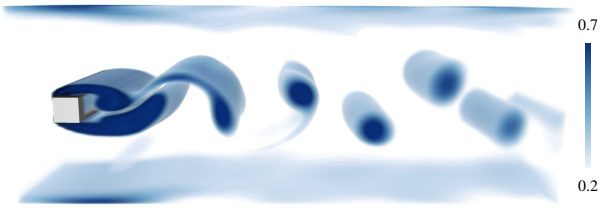

(e) Objective vorticity in Eq. (96) by Günther et al [GGT17].

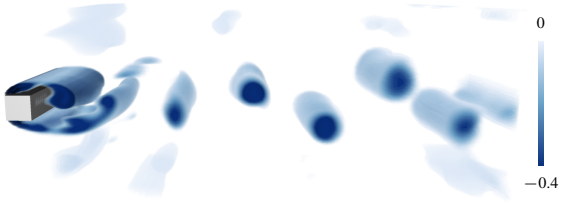

(f) Objective λ_2 in Eq. (97) by Günther et al [GGT17].

Figure 14: In the SQUARE CYLINDER flow of Camarri et al. [CSBI05], objective region-based measures should be similar to traditional Galilean invariant measures, since vortices translates with almost equal speed. λ_2 based on the relative vorticity tensor (a) is not consistent with traditional λ_2, and M_z (b) produces false-positives, whereas IVD (c), LAVD (d), and vorticity (e) and λ_2 (f) in the optimal reference frames detect the von Kármán vortex street well.

the coefficients A, B, C, D of a quartic polynomial

$$p^4 + Ap^3 + Bp^2 + Cp + D \tag{78}$$

which has roots in the range $[-1,1]$ if $\mathbf{M}$ is indefinite. Along particle trajectories, the binary value ($\mathbf{M}$ is indefinite or not) is averaged to find trajectories that stay in indefinite areas for a long time, assuming that long-term non-hyperbolic behavior is an indicator for a vortex. An example of the M_z measure is given in Fig. 14b. Sahner et al. [SWTH07] extracted strain skeletons and extremal lines of M_z.

Vorticity-based Measures. Some objective measures were derived from vorticity. Note that vorticity itself is not objective, as document for instance in [Ast79,HHFH16]. Haller et al. [HHFH16] derived a method from a dynamic polar decomposition of the deformation gradient. Aside from anchoring it deeply in continuum dynamics, it led to an interesting observation: any subtraction of two vorticity values $\boldsymbol{\omega}(\mathbf{x}_1,t) - \boldsymbol{\omega}(\mathbf{x}_2,t)$ will cancel out the spatially-constant rotation rate of the reference frame, if the vorticity was sampled at the same time t. This means, every subtraction of two vorticity values is objective–including spatial derivatives. For this reason, the location of vorticity extrema [SKA99] is objective, as well. In both 2D and 3D, Haller et al. [HHFH16] subtracted the spatial mean of vorticity $\boldsymbol{\omega}_{avg}$ in a local neighborhood $U \subseteq D$:

$$\boldsymbol{\omega}_{avg}(t) = \frac{1}{|U(t)|} \int_{U(t)} \boldsymbol{\omega}(\mathbf{x},t)\, \mathrm{d}V \tag{79}$$

where $|U(t)|$ is the area or volume of $U(t)$ and $\mathrm{d}V$ denotes an area or volume element, respectively. Using Eq. (79), they defined the instantaneous vorticity deviation (IVD) as the difference in vorticity at a point to the average of its local neighborhood:

$$\mathrm{IVD}(\mathbf{x},t) = |\boldsymbol{\omega}(\mathbf{x},t) - \boldsymbol{\omega}_{avg}(t)| \tag{80}$$

Fig. 14c gives an example. A Lagrangian extension that considers the temporal evolution is the Lagrangian-averaged vorticity deviation (LAVD), which is computed by integrating IVD for duration τ along a pathline $\mathbf{c}(t)$ that was seeded at $(\mathbf{x},t_0)$:

$$\mathrm{LAVD}^{\tau}_{t_0}(\mathbf{x}) = \int_{t_0}^{t_0+\tau} |\boldsymbol{\omega}(\mathbf{c}(t),t) - \boldsymbol{\omega}_{avg}(t)|\, \mathrm{d}t \tag{81}$$

See Fig. 14d for an example. Both IVD and LAVD are objective, see Haller et al. [HHFH16], but note that these measures are *relative* to their neighborhood and that their value-range depends on the neighborhood size $U(t)$. Even though these vorticity-based measures are gracefully objective (including the location of extrema), vorticity may produce false-positives in shear flow [Rob91]. These can be filtered by observing closed iso-contours with a significant

maximum inside to exclude noise. Lugt [Lug79] noted that a local vorticity extremum is not necessary for the existence of a vortex.

5.6. Reference Frame Selection by Flow Decomposition

Aside from the definition of extraction methods that are invariant under certain types of reference frame motion (Galilean invariance, objectivity, rotation invariance), there is a thread of research on finding a suitable reference frame in which the flow appears (nearly) steady.

A naïve approach is to split the unsteady flow $\mathbf{v}$ into a mean flow $\mathbf{v}_{avg}$ and a residual fluctuation $\mathbf{v}'$, i.e.:

$$\mathbf{v} = \mathbf{v}_{avg} + \mathbf{v}' \tag{82}$$

and to analyze the fluctuation $\mathbf{v}'$ only. We can thereby distinguish between the computation of a temporal mean and a spatial mean. The temporal mean is used in the *Reynolds* decomposition [Rey94], which is frequently used for turbulence studies [SB90]. The ambient motion can also be estimated as the spatial mean of the velocity around a given point. For some simple flow configurations, such as a von-Kármán vortex street, a certain percentage of the inflow velocity can be used instead, which must be known by domain experience [WSTH07]. If the value is chosen correctly, the resulting flow becomes near-steady in most parts of the domain (though not everywhere). Note that neither temporal nor spatial mean subtraction guarantees that the flow ends up in a near-steady reference frame.

More sophisticated reference frame choices use decompositions of the flow to find a harmonic vector field [Wie04], cf. Eq. (12), that can be subtracted to eliminate the general motion. The idea behind this is that harmonic fields are divergence-free and curl-free, and thus the subtraction of this fields preserves the local divergence and rotation properties. The Helmholtz-Hodge decomposition (HHD) [BNPB13] decomposes a vector field into a scalar potential $-\nabla\phi$ (curl-free), a vector potential $\nabla \times \boldsymbol{\psi}$ (divergence-free) and a harmonic vector field $\mathbf{h}$:

$$\mathbf{v} = \underbrace{-\nabla\phi}_{\text{curl-free}} + \underbrace{\nabla \times \boldsymbol{\psi}}_{\text{divergence-free}} + \underbrace{\mathbf{h}}_{\text{harmonic}} \tag{83}$$

If a harmonic part is present, the resulting components and the uniqueness of the decomposition strongly depend on the boundary conditions. Bhatia et al. [BPKB14] used their *natural* HHD to extract vortices in the resulting (near-)steady flow. Note that a harmonic part cannot capture rotational transport, as it is always irrotational. Aside from using the HHD to perform a change of the reference frame, vortices have also been characterized as extremal structures of the magnitude of the vector potential, e.g., by Tong et al. [TLHD03] and Wiebel et al. [Wie04].

Recently, Bujack et al. [BHJ16] proposed to find critical points by locally adjusting the frame of reference to the most persistent one. For this, they analyzed the extrema of the determinant of $\mathbf{J}$ by finding critical points in its gradient field and classifying them by the Hessian H:

$$\nabla(det(\mathbf{J})) = \mathbf{0} \;\wedge\; H(det(\mathbf{J})) \text{ is positive definite} \tag{84}$$

Note that in 2D, $Q = det(\mathbf{J})$, cf. Eq. (21), thus their method searches for extrema in the second invariant of the Jacobian matrix, which can be seen as searching for extrema in the 2D counterpart to the Q-criterion, i.e., the Okubo-Weiss criterion. Unlike the previous Galilean invariant methods, the approach of Bujack et al. [BHJ16] does not involve temporal derivatives and is therefore not equivalent to Weinkauf et al. [WSTH07] or Fuchs et al. [FPH*08]. The Hessian in Eq. (84) involves third-order spatial derivatives, which has implications on the numerical robustness.

5.7. Optimal Local Reference Frames

Lugt [Lug79] noted that in unsteady flows there is no *global* reference frame in which the entire flow appears steady, since individual features move at different speeds and in possibly different directions. In a similar sense, Perry and Chong [PC94] noted that for certain flows, e.g., jets in cross-flow, vortices accelerate and become steady in different frames.

Objectivity. For these reasons, Günther et al. [GGT17] did not seek for a global (spatially-constant) reference frame, but for a *local* one. They estimated an optimal local reference frame for every point $(\mathbf{x},t)$, in which the transformed velocity field is as steady as possible in a local neighborhood U around $(\mathbf{x},t)$. In other words, they minimized the temporal derivative of the transformed field:

$$\int_U \|\mathbf{v}_t^*\|^2 dV \rightarrow \min. \tag{85}$$

They have shown that the temporal derivative of the transformed velocity field $\mathbf{v}_t^*$ can be equivalently expressed as follows:

$$\mathbf{v}_t^* = \mathbf{Q}\,(\mathbf{v}_t - \mathbf{M}\,\mathbf{u}). \tag{86}$$

Thereby, the parameters of the optimal reference frame are contained in vector $\mathbf{u}$. In 2D, $\mathbf{u}$ is a 6-vector and in 3D, $\mathbf{u}$ is a 12-vector. In 2D, $\mathbf{M}$ is a 2×6 matrix and in 3D, $\mathbf{M}$ is a 3×12 matrix:

$$2D: \quad \mathbf{M} = (-\mathbf{J}\,\mathbf{x}_p + \mathbf{v}_p \;,\; \mathbf{J} \;,\; \mathbf{x}_p \;,\; \mathbf{I}) \tag{87}$$

$$3D: \quad \mathbf{M} = (-\mathbf{J}\,\mathbf{X} + \mathbf{V} \;,\; \mathbf{J} \;,\; \mathbf{X} \;,\; \mathbf{I}) \tag{88}$$

with $\mathbf{x}_p = (-y,x)^{\mathrm{T}}$, $\mathbf{v}_p = (-v,u)^{\mathrm{T}}$, $\mathbf{X} = sk(\mathbf{x})$, $\mathbf{V} = sk(\mathbf{v})$. Eq. (86) shows that the vector field and the reference frame are completely separated: $\mathbf{M}$ contains only $\mathbf{v}$ and its derivatives, while all information of the frame is stored in $\mathbf{u}$.

Eq. (85) is minimized using Eq. (86), which can be written as the solution of the linear system

$$\widehat{\mathbf{M}}\,\mathbf{u} = \widehat{\mathbf{y}} \tag{89}$$

$$\text{with} \quad \widehat{\mathbf{M}} = \int_U \mathbf{M}^{\mathrm{T}}\mathbf{M}\,dV \quad , \quad \widehat{\mathbf{y}} = \int_U \mathbf{M}^{\mathrm{T}}\mathbf{v}_t\,dV. \tag{90}$$

Let $\widetilde{\mathbf{u}} = (\widetilde{\mathbf{u}}_1, \widetilde{\mathbf{u}}_2, \widetilde{\mathbf{u}}_3, \widetilde{\mathbf{u}}_4)^{\mathrm{T}} = \widehat{\mathbf{M}}^{-1}\,\widehat{\mathbf{y}}$ be the solution of Eq. (89). Then, the new fields in the locally optimal reference frame are

$$\widetilde{\mathbf{v}} = \mathbf{v} + sk(\widetilde{\mathbf{u}}_1)\,\mathbf{x} + \widetilde{\mathbf{u}}_2 \tag{91}$$

$$\widetilde{\mathbf{J}} = \mathbf{J} + sk(\widetilde{\mathbf{u}}_1) \tag{92}$$

$$\widetilde{\mathbf{v}}_t = \mathbf{v}_t - \mathbf{M}\,\widetilde{\mathbf{u}} \tag{93}$$

$$\widetilde{\mathbf{a}} = \widetilde{\mathbf{J}}\,\widetilde{\mathbf{v}} + \widetilde{\mathbf{v}}_t. \tag{94}$$

Note that $\widetilde{\mathbf{u}}_1$ and $\widetilde{\mathbf{u}}_3$ are scalars in 2D, namely the first-order and second-order derivative of the angular velocity of the rotation of the reference frame.

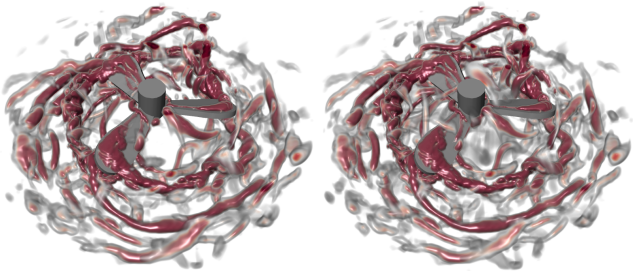

(a) Standard λ_2 [JH95]. (b) Objective $\widetilde{\lambda}_2$ [GGT17].

Figure 15: Comparison of the original Galilean invariant λ_2 measure by Jeong and Hussain [JH95] with the objective version of Günther et al. [GGT17]. The differences are in the details. The dominant structures are recovered with both methods similarly.

Günther et al. [GGT17] limited the reference frame transformation to rotations and translations. For any rotation and translation of the reference frame that can be applied to the input vector field, their method computes the same distinguished local reference frame. All techniques applied in this frame, therefore become independent of rotations and translations of the input. Thus, any vortex measure that is applied in the optimal frame using Eqs. (91)–(94) becomes objective.

Vortex Definition in the Optimal Frame. In the optimal reference frame that was described in Section 5.7, standard vortex extraction methods directly become frame invariant, i.e., objective. In 2D, optimal vortex corelines appear as paths of critical points in $\widetilde{\mathbf{v}}$ and in 3D, optimal vortex corelines are extracted by parallel vectors:

$$\text{2D: } \widetilde{\mathbf{v}} = \mathbf{0} \qquad \text{3D: } \widetilde{\mathbf{J}}\widetilde{\mathbf{v}} \parallel \widetilde{\mathbf{v}} \quad . \tag{95}$$

Note that these techniques usually only work in steady flows. Since Günther et al. [GGT17] observe the unsteady flows in the optimal near-steady reference frame, their method extracts vortex corelines of pathlines. See Fig. 8d for an example.

In contrast to the relative vorticity tensor of Drouot and Lucius [DL76] in Eq. (70), Günther et al. [GGT17] proposed a new objective vorticity tensor $\widetilde{\mathbf{\Omega}}$ that views vorticity in the optimal reference frame. Based on this, they defined an objective counterpart to the 2D and 3D vorticity as:

$$\text{2D: } \widetilde{\omega} = ap(\widetilde{\mathbf{J}}) \qquad \text{3D: } \widetilde{\boldsymbol{\omega}} = ap(\widetilde{\mathbf{J}}) \quad . \tag{96}$$

An example of the objective vorticity is shown in Fig. 14e.

They also defined a new objective $\widetilde{\lambda}_2$ measure, which is shown in Fig. 14f:

$$\widetilde{\lambda}_2(\mathbf{S}^2 + \widetilde{\mathbf{\Omega}}^2) < 0 \qquad \text{with} \qquad \widetilde{\mathbf{\Omega}} = \frac{\widetilde{\mathbf{J}} - \widetilde{\mathbf{J}}^{\mathrm{T}}}{2} \quad . \tag{97}$$

Aside from using λ_2 and Q, other vortex measures can be similarly applied in the optimal reference frame.

The optimization-based approaches require a linear optimization, which has numerical consequences and higher computational cost than traditional techniques [GGT17]. The techniques do, however, contain an inherent smoothing due to the finite neighborhood size U, which results in more stable and smoother vortex corelines. It should be noted, though, that higher reference frame invariances are not always that much different compared to the results of traditional Galilean invariant techniques. Fig. 15 gives an example in a numerical simulation of a rotating mixer. Especially, when the unsteadiness is low (the temporal derivative has much smaller magnitude than the spatial derivatives) or when vortices are in fact moving with almost equal speed on nearly linear paths, such as in the von-Kármán vortex street.

5.8. Extraction of Vortex Boundaries

Aside from finding vortex corelines, the size of vortices is also of interest. With region-based methods, the size is determined by a threshold, which is typically difficult to set. Line-based methods may serve as a starting point for region growing approaches. For instance, Banks and Singer [BS95] grow vortex tubes from their corelines in the plane that is orthogonal to the coreline until a vorticity or pressure threshold is violated. Starting from a coreline, Garth et al. [GTS*04] consider a vortex tube radius optimal if the tangential velocity on the circular tube boundary is maximized. This approach is motivated by the Rankine vortex model, which models the decay of the tangential velocity. For a closed flow domain, Lagerstrom [Lag75] considered a vortex to be the maximal set of nested closed streamlines. Petz et al. [PKPH09] formed a hierarchy of closed streamlines to define vortex hierarchies. Wischgoll et al. [WSH01] and Tricoche et al. [TWSH02] tracked closed streamlines over time, which has limited meaning for unsteady fluid flows, since streamlines topology does not represent pathline behavior. Note that all streamline-based approaches highly depend on the chosen reference frame. Starting from an extracted coreline, Bauer et al. [BPSS02] grew the vortex core region until the imaginary part of the complex-conjugate eigenvalues of $\mathbf{J}$ fell below a certain threshold, cf. Eq. (42). In recent years, Lagrangian Coherent Structures (LCS) [Hal15] have been computed objectively using calculus of variations. LCSs are distinguished material curves that organize the flow. A subclass are elliptic LCS, which preserve arc length and area in incompressible 2D flows. Haller [Hal15] considered the outermost elliptic LCS, of a family of nested elliptic LCSs, as the boundary of a coherent vortex. Serra and Haller [SH16b] used the variational framework to find objective Eulerian vortex boundaries as closed instantaneous (per time step) curves across which the averaged material stretching rate shows no leading-order variability. Based on these (instantaneous) curves, they forecasted the Lagrangian persistence of a vortex [SH16a].

5.9. Vorticity Transport

Related to the visualization of vortices is the visualization of vorticity transport, which was studied in order to understand the role of vorticity in the development and evolution of vortices. Based on the incompressible Navier-Stokes momentum equations with uniform density and viscosity, the vorticity transport is described as follows, cf. Batchelor [Bat00]:

$$\frac{\partial \boldsymbol{\omega}}{\partial t} + \mathbf{u} \cdot \nabla \boldsymbol{\omega} = \boldsymbol{\omega} \cdot \nabla \mathbf{v} + \nu \nabla^2 \boldsymbol{\omega} \tag{98}$$

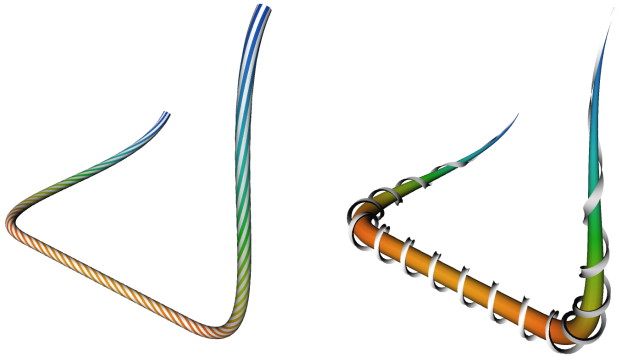

Figure 16: Iconic illustration of vortices by Sahner et al. [SWH05a], which shows swirling strength by color and width, in addition to a visualization of twist by spiral patterns or orbiting lines. © Eurographics 2005

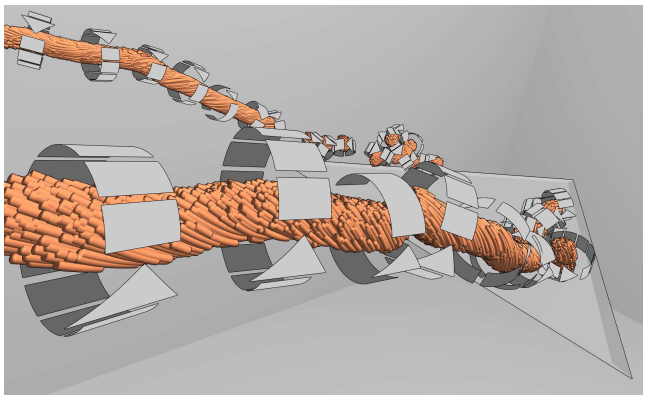

Figure 17: Illustration of rotation direction, rotation strength and spatial extent of a vortex by Shafii et al. [SOK*13] at the example of a delta wing. © Eurographics 2013

where ν is the kinematic viscosity. Sadlo et al. [SPS06] decomposed the first term on the right hand side into a parallel and an orthogonal part:

$$\frac{\partial \boldsymbol{\omega}}{\partial t} + \mathbf{u} \cdot \nabla \boldsymbol{\omega} = \underbrace{(\boldsymbol{\omega} \cdot \nabla \mathbf{v})_{\parallel \boldsymbol{\omega}}}_{\text{stretching}} + \underbrace{(\boldsymbol{\omega} \cdot \nabla \mathbf{v})_{\perp \boldsymbol{\omega}}}_{\text{tilting}} + \underbrace{\nu \nabla^2 \boldsymbol{\omega}}_{\text{diffusion}} \tag{99}$$

and visualized the stretching, tilting and diffusion along pathlines, which gave deeper insight into vortex dynamics, revealing how vorticity and vortices are reinforced or weakened by the flow field. We refer to [SPS06] for an extension to non-uniformly viscous flow. To study the interaction of shear and vortices in unsteady flows, Schafhitzel et al. [SBV*11] extracted and visualized shear layers.

5.10. Vortex Verification and Visualization

Orthogonal to vortex definitions are the verification of numerical extraction results and their further processing for visualization. Jiang et al. [JMT02a] presented a method to verify corelines based on the geometry of streamlines.

Corelines should ideally be pathlines, since then they would represent particles that other particles swirl around. For unsteady 2D flows, the *tangent alignment* of a coreline $\mathbf{c}(t)$ is a scalar line attribute that is defined as the absolute value of the dot product between (space-time) vector field $\overline{\mathbf{p}}$ and the tangent of the space-time coreline $\overline{\mathbf{c}}(t) = (\mathbf{c}(t), t)^{\mathrm{T}}$:

$$\left| \frac{\overline{\mathbf{p}}(\overline{\mathbf{c}}(t), t)}{\|\overline{\mathbf{p}}(\overline{\mathbf{c}}(t), t)\|} \cdot \frac{\mathrm{d}\overline{\mathbf{c}}(t)/\mathrm{d}t}{\|\mathrm{d}\overline{\mathbf{c}}(t)/\mathrm{d}t\|} \right| \tag{100}$$

This measure can serve for comparisons between different coreline techniques [GST16], see Fig. 10 for an example. In unsteady 3D flows, vortex corelines sweep over a surface in space-time. Ideally, the normal of this surface should be orthogonal to the flow direction.

Sadarjoen and Post [SP99] fit ellipses to depict streamline-based vortices in 2D. To improve the vortex core visualization in 3D, Garth et al. [GTS*04] computed hull surfaces around vortex cores based on the Rankine vortex model, which reveals surfaces on which the tangential velocity is maximized. Sahner et al. [SWH05a] proposed an iconic representation to indicate vortex scale and extent, which is shown in Fig. 16. Vortex corelines visualizations are frequently augmented with spiraling pathlines [WSTH07]. Shafii et al. [SOK*13] encoded rotation direction, rotational strength and the spatial extent of vortex cores and show the behavior of the flow in the vicinity of the vortex. An example is shown in Fig. 17.

6. Conclusion and Future Work

In this report, we summarized the established and recent work in the area of vortex extraction in fluid flows. We covered common region-based and line-based approaches, geometric and integration-based methods, recent objective techniques, flow decomposition and reference frame selections.

Despite decades of research that were spent on this subject, there are still a number of open problems:

- Most region-based vortex extractors are Eulerian, i.e., they only reflect characteristics of a single time step. In order to capture the transient effects of the fluids, Eulerian measures can be accumulated along pathlines, which leads to Lagrangian scalar fields. These fields can be expensive to compute and render.
- Many region-based standard techniques such as Q and λ_2 are based on the assumption that the flow is steady and incompressible. It is not always clear how these methods can be cleanly extended to unsteady or compressible flows.
- Vorticity produces false-positives in shear flow. At present, there is a clear lack in techniques that handle flows that are dominated by shear.
- Most vortex characterizations are local and are biased if the flow is formed as a sum of turbulent motion of multiple scales. How can vortex cascades be extracted?
- Early on, scientists emphasized the relevance of an appropriate reference frame to observe the flow structures. Is the right reference frame found yet and are the extraction approaches the most-suitable and efficient ones?

- Which reference frame invariance makes sense in practice? There is a long ongoing debate, whether Galilean invariance is sufficient or whether the computationally more expensive objective techniques should be preferred. So far, there is no universal answer and the choice depends heavily on the data at hand.
- Line-based vortex extractors are still not robust enough and stable enough. The line geometry is often segmented into pieces and requires filtering and post-processing. A more stable extractor that deals with numerical problems would be very welcome.
- To achieve better adaption into practice, more standardization and reference implementations are necessary.
- Better benchmark and testing grounds are needed to compare and evaluate the newly-appearing vortex extractors.
- Many vortex definitions still await an extension to uncertain data.

Vortex extraction remains an active field of research. We look forward to the advances that we will see in the future.

Acknowledgements

The visualizations in Figs. 6, 7, 8 and 14 were rendered with the visualization toolkit Amira [SWH05b].

References

[Ast79] ASTARITA G.: Objective and generally applicable criteria for flow classification. *Journal of Non-Newtonian Fluid Mechanics 6*, 1 (1979), 69–76. 8, 15, 16

[Bat00] BATCHELOR G. K.: *An introduction to Fluid Dynamics*. Cambridge university press, 2000. 18

[BCP*12] BRAMBILLA A., CARNECKY R., PEIKERT R., VIOLA I., HAUSER H.: Illustrative flow visualization: State of the art, trends and challenges. In *Eurographics 2012 State of the Art Reports (STARs)* (Cagliari, Italy, 2012), pp. 75–94. 1

[BHD*15] BISWAS A., HE W., DENG Q., CHEN C.-M., SHEN H.-W., MACHIRAJU R., RANGARAJAN A.: An uncertainty-driven approach to vortex analysis using oracle consensus and spatial proximity. In *Proc. IEEE Pacific Visualization Symposium* (Hangzhou, China, 2015), pp. 223–230. 8, 11

[BHJ16] BUJACK R., HLAWITSCHKA M., JOY K. I.: Topology-inspired Galilean invariant vector field analysis. In *IEEE Pacific Visualization Symposium* (Taipei, Taiwan, April 2016), pp. 72–79. 8, 17

[BKC*13] BORGO R., KEHRER J., CHUNG D. H. S., MAGUIRE E., LARAMEE R. S., HAUSER H., WARD M., CHEN M.: Glyph-based visualization: Foundations, design guidelines, techniques and applications. In *Eurographics State of the Art Reports (STARs)* (Girona, Spain, 2013), pp. 39–63. 1

[BNPB13] BHATIA H., NORGARD G., PASCUCCI V., BREMER P.-T.: The Helmholtz-Hodge decomposition–A survey. *IEEE Transactions on Visualization and Computer Graphics 19*, 8 (2013), 1386–1404. 3, 8, 17

[BP02] BAUER D., PEIKERT R.: Vortex tracking in scale-space. In *Proc. Symposium on Data Visualisation* (Barcelona, Spain, 2002), pp. 233–240. 8, 12

[BPKB14] BHATIA H., PASCUCCI V., KIRBY R. M., BREMER P.-T.: Extracting features from time-dependent vector fields using internal reference frames. *Computer Graphics Forum (Proc. EuroVis) 33*, 3 (2014), 21–30. 17

[BPSS02] BAUER D., PEIKERT R., SATO M., SICK M.: A case study in selective visualization of unsteady 3d flow. In *Proceedings of the Conference on Visualization'02* (2002), IEEE Computer Society, pp. 525–528. 18

[BS90] BLACKWELDER R. F., SWEARINGEN J. D.: The role of inflectional velocity profiles in wall bounded flows. *Near-Wall Turbulence* (1990), 268–288. 9

[BS95] BANKS D. C., SINGER B. A.: A predictor-corrector technique for visualizing unsteady flow. *IEEE Transactions on Visualization and Computer Graphics 1* (1995), 151–163. 8, 14, 18

[CBA05] CHAKRABORTY P., BALACHANDAR S., ADRIAN R. J.: On the relationships between local vortex identification schemes. *Journal of Fluid Mechanics 535* (2005), 189–214. 8, 10, 11, 15

[CL93] CABRAL B., LEEDOM L.: Imaging vector fields using line integral convolution. *Computer Graphics (Proc. SIGGRAPH) 27* (1993), 263–272. 1, 4

[CML*07] CHEN G., MISCHAIKOW K., LARAMEE R. S., PILARCZYK P., ZHANG E.: Vector field editing and periodic orbit extraction using morse decomposition. *IEEE Transactions on Visualization and Computer Graphics 13*, 4 (2007), 769–785. 4

[CPC90] CHONG M. S., PERRY A. E., CANTWELL B. J.: A general classification of three-dimensional flow fields. *Physics of Fluids A: Fluid Dynamics 2*, 5 (1990), 765–777. 8, 10, 15

[CQB99] CUCITORE R., QUADRIO M., BARON A.: On the effectiveness and limitations of local criteria for the identification of a vortex. *European Journal of Mechanics - B/Fluids 18*, 2 (1999), 261–282. 8, 9, 10, 15

[CSBI05] CAMARRI S., SALVETTI M.-V., BUFFONI M., IOLLO A.: Simulation of the three-dimensional flow around a square cylinder between parallel walls at moderate Reynolds numbers. In *XVII Congresso di Meccanica Teorica ed Applicata* (Genova, Italy, 2005). 16

[CSSdS07] CHELTON D. B., SCHLAX M. G., SAMELSON R. M., DE SZOEKE R. A.: Global observations of large oceanic eddies. *Geophysical Research Letters 34*, 15 (2007). 1

[DD00] DUBIEF Y., DELCAYRE F.: On coherent-vortex identification in turbulence. *Journal of Turbulence 1*, 1 (2000), 011–011. 10

[DL76] DROUOT R., LUCIUS M.: Approximation du second ordre de la loi de comportement des fluides simples. lois classiques déduites de l'introduction d'un nouveau tenseur objectif. *Archiwum Mechaniki Stosowanej 28*, 2 (1976), 189–198. 8, 15, 18

[dLvL99] DE LEEUW W., VAN LIERE R.: Collapsing flow topology using area metrics. In *Proceedings of the Conference on Visualization* (1999), VIS '99, pp. 349–354. 5

[DT92] DRESSELHAUS E., TABOR M.: The kinematics of stretching and alignment of material elements in general flow fields. *Journal of Fluid Mechanics 236* (1992), 415–444. 15

[ELC*12] EDMUNDS M., LARAMEE R. S., CHEN G., MAX N., ZHANG E., WARE C.: Surface-based flow visualization. *Computers & Graphics 36*, 8 (2012), 974–990. 1

[EW10] EFFENBERGER F., WEISKOPF D.: Finding and classifying critical points of 2D vector fields: A cell-oriented approach using group theory. *Computing and Visualization in Science 13*, 8 (Dec. 2010), 377–396. 5

[FPH*08] FUCHS R., PEIKERT R., HAUSER H., SADLO F., MUIGG P.: Parallel vectors criteria for unsteady flow vortices. *IEEE Transactions on Visualization and Computer Graphics 14*, 3 (2008), 615–626. 8, 12, 17

[FPS*08] FUCHS R., PEIKERT R., SADLO F., ALSALLAKH B., GRÖLLER M. E.: Delocalized unsteady vortex region detectors. In *Proc. Vision, Modeling and Visualization* (Konstanz, Germany, 2008), pp. 81–90. 8, 15

[FWT08] FREDERICH O., WASSEN E., THIELE F.: Prediction of the flow around a short wall-mounted cylinder using LES and DES. *Journal of Numerical Analysis, Industrial and Applied Mathematics (JNAIAM) 3*, 3-4 (2008), 231–247. 9

[GG17] GÜNTHER T., GROSS M.: Flow-induced inertial steady vector field topology. *Computer Graphics Forum (Proc. Eurographics) 36*, 2 (2017), 143–152. 5

[GGT17] GÜNTHER T., GROSS M., THEISEL H.: Generic objective vortices for flow visualization. *ACM Transactions on Graphics (Proc. SIGGRAPH) 36*, 4 (2017), 141:1–141:11. 6, 7, 8, 11, 16, 17, 18

[GLL91] GLOBUS A., LEVIT C., LASINSKI T.: A tool for visualizing the topology of three-dimensional vector fields. In *Proc. IEEE Visualization* (1991), pp. 33–40. 5, 6, 8, 11, 14

[GLT*07] GARTH C., LARAMEE R. S., TRICOCHE X., SCHNEIDER J., HAGEN H.: Extraction and visualization of swirl and tumble motion from engine simulation data. In *Topology-based Methods in Visualization*, Visualization and Mathematics. Springer Berlin Heidelberg, 2007, pp. 121–135. 1, 11

[GMG01] GRAFTIEAUX L., MICHARD M., GROSJEAN N.: Combining PIV, POD and vortex identification algorithms for the study of unsteady turbulent swirling flows. *Measurement Science and Technology 12*, 9 (2001), 1422. 8, 10

[GST16] GÜNTHER T., SCHULZE M., THEISEL H.: Rotation invariant vortices for flow visualization. *IEEE Transactions on Visualization and Computer Graphics (Proc. IEEE SciVis 2015) 22*, 1 (2016), 817–826. 6, 7, 8, 11, 12, 13, 19

[GT16] GÜNTHER T., THEISEL H.: Inertial steady 2D vector field topology. *Computer Graphics Forum (Proc. Eurographics) 35*, 2 (2016), 455–466. 5

[GTS*04] GARTH C., TRICOCHE X., SALZBRUNN T., BOBACH T., SCHEUERMANN G.: Surface techniques for vortex visualization. In *Proc. Joint Eurographics - IEEE TCVG Conference on Visualization (VISSYM)* (Konstanz, Germany, 2004), Eurographics Association, pp. 155–164. 8, 18, 19

[Gün16] GÜNTHER T.: *Opacity Optimization and Inertial Particles in Flow Visualization*. PhD thesis, University of Magdeburg, June 2016. 3, 4, 7

[Hal05] HALLER G.: An objective definition of a vortex. *Journal of Fluid Mechanics 525* (2005), 1–26. 7, 8, 13, 15, 16

[Hal15] HALLER G.: Lagrangian coherent structures. *Annual Review of Fluid Mechanics 47* (2015), 137–162. 7, 8, 18

[HH89] HELMAN J. L., HESSELINK L.: Representation and display of vector field topology in fluid flow data sets. *Computer 22*, 8 (1989), 27–36. 3, 5

[HH91] HELMAN J. L., HESSELINK L.: Visualizing vector field topology in fluid flows. *IEEE Computer Graphics and Applications 11* (May 1991), 36–46. 1, 3, 5

[HH16] HADJIGHASEM A., HALLER G.: Geodesic transport barriers in jupiter's atmosphere: A video-based analysis. *SIAM Review 58*, 1 (2016), 69–89. 1

[HHFH16] HALLER G., HADJIGHASEM A., FARAZMAND M., HUHN F.: Defining coherent vortices objectively from the vorticity. *Journal of Fluid Mechanics 795* (2016), 136–173. 7, 8, 16

[HK98] HUA B. L., KLEIN P.: An exact criterion for the stirring properties of nearly two-dimensional turbulence. *Physica D: Nonlinear Phenomena 113*, 1 (1998), 98–110. 8, 10

[HLH*16] HEINE C., LEITTE H., HLAWITSCHKA M., IURICICH F., DE FLORIANI L., SCHEUERMANN G., HAGEN H., GARTH C.: A survey of topology-based methods in visualization. *Computer Graphics Forum 35*, 3 (2016), 643–667. 1, 4, 6

[HMK98] HUA B. L., MCWILLIAMS J. C., KLEIN P.: Lagrangian accelerations in geostrophic turbulence. *Journal of Fluid Mechanics 366* (1998), 87–108. 8, 10

[Hun87] HUNT J. C. R.: Vorticity and vortex dynamics in complex turbulent flows. *Transactions on Canadian Society for Mechanical Engineering (Proc. CANCAM) 11*, 1 (1987), 21–35. 8, 9, 10, 13

[Hus86] HUSSAIN A. F.: Coherent structures and turbulence. *Journal of Fluid Mechanics 173* (1986), 303–356. 10

[HWM88] HUNT J. C. R., WRAY A. A., MOIN P.: Eddies, streams, and convergence zones in turbulent flows. In *Studying Turbulence Using Numerical Simulation Databases, 2* (Dec. 1988). 8, 9, 10

[JCWD14] JU T., CHENG M., WANG X., DUAN Y.: A robust parity test for extracting parallel vectors in 3D. *IEEE Transactions on Visualization and Computer Graphics (Proc. IEEE SciVis) 20*, 12 (2014), 2526–2534. 6

[JH95] JEONG J., HUSSAIN F.: On the identification of a vortex. *Journal of Fluid Mechanics 285* (1995), 69–94. 7, 8, 9, 10, 13, 18

[JMT02a] JIANG M., MACHIRAJU R., THOMPSON D.: Geometric verification of swirling features in flow fields. In *Proc. IEEE Visualization* (Boston, Massachusetts, USA, 2002), pp. 307–314. 19

[JMT02b] JIANG M., MACHIRAJU R., THOMPSON D.: A novel approach to vortex core region detection. In *Proc. Symposium on Data Visualisation (VISSYM)* (Barcelona, Spain, 2002), pp. 217–226. 8, 11

[KGP*13] KÖHLER B., GASTEIGER R., PREIM U., THEISEL H., GUTBERLET M., PREIM B.: Semi-automatic vortex extraction in 4D PC-MRI cardiac blood flow data using line predicates. *IEEE Transactions on Visualization and Computer Graphics (Proc. IEEE SciVis) 19*, 12 (2013), 2773–2782. 1

[KH97] KENWRIGHT D., HAIMES R.: Vortex identification – Applications in aerodynamics: A case study. In *Proceedings of the 8th Conference on Visualization '97* (Los Alamitos, CA, USA, 1997), VIS '97, IEEE Computer Society Press, pp. 413–ff. 1, 11, 13, 14

[KHNH11] KASTEN J., HOTZ I., NOACK B. R., HEGE H.-C.: On the extraction of long-living features in unsteady fluid flows. In *Topological Methods in Data Analysis and Visualization*, Mathematics and Visualization. Springer, 2011, pp. 115 – 126. 12

[KHNH12] KASTEN J., HOTZ I., NOACK B. R., HEGE H.-C.: Vortex merge graphs in two-dimensional unsteady flow fields. In *EuroVis - Short Papers* (Vienna, Austria, 2012), Eurographics Association, pp. 1–5. 11

[KMM87] KIM J., MOIN P., MOSER R.: Turbulence statistics in fully developed channel flow at low Reynolds number. *Journal of fluid mechanics 177* (1987), 133–166. 9

[Kol07] KOLÁŘ V.: Vortex identification: New requirements and limitations. *International journal of heat and fluid flow 28*, 4 (2007), 638–652. 11

[KRHH11] KASTEN J., REININGHAUS J., HOTZ I., HEGE H.-C.: Two-dimensional time-dependent vortex regions based on the acceleration magnitude. *IEEE Transactions on Visualization and Computer Graphics (Proc. IEEE SciVis) 17*, 12 (2011), 2080–2087. 8, 11, 12

[Lag75] LAGERSTROM P. A.: Solutions of the Navier–Stokes equation at large Reynolds number. *SIAM Journal on Applied mathematics 28*, 1 (1975), 202–214. 8, 18

[LCJK*09] LARAMEE R. S., CHEN G., JANKUN-KELLY M., ZHANG E., THOMPSON D.: Bringing topology-based flow visualization to the application domain. In *Topology-Based Methods in Visualization II*. Springer, 2009, pp. 161–176. 5

[LDG98] LÖFFELMANN H., DOLEISCH H., GRÖLLER E.: Visualizing dynamical systems near critical points. In *In Spring Conference on Computer Graphics and its Applications* (1998), pp. 175–184. 6

[LEG*08] LARAMEE R. S., ERLEBACHER G., GARTH C., THEISEL H., TRICOCHE X., WEINKAUF T., WEISKOPF D.: Applications of texture-based flow visualization. *Engineering Applications of Computational Fluid Mechanics (EACFM) 2*, 3 (2008), 264–274. 1

[LHD*04] LARAMEE R. S., HAUSER H., DOLEISCH H., VROLIJK B., POST F. H., WEISKOPF D.: The state of the art in flow visualization: Dense and texture-based techniques. *Computer Graphics Forum 23*, 2 (2004), 203–221. 1

[LHZP07] LARAMEE R. S., HAUSER H., ZHAO L., POST F. H.: Topology-based flow visualization, the state of the art. In *Topology-based Methods in Visualization*, Mathematics and Visualization. Springer Berlin Heidelberg, 2007, pp. 1–19. 1, 6

[LRR00] LODHA S., RENTERIA J., ROSKIN K.: Topology preserving compression of 2D vector fields. In *In Proc. IEEE Visualization* (Salt Lake City, Utah, USA, 2000), pp. 343–350. 4

[LSD90] LEVY Y., SEGINER A., DEGANI D.: Graphical visualization of vortical flows by means of helicity. *AIAA journal 28*, 8 (1990), 1347–1352. 8, 10

[Lug79] LUGT H. J.: The dilemma of defining a vortex. In *Recent developments in theoretical and experimental fluid mechanics*. Springer, 1979, pp. 309–321. 1, 6, 9, 17

[Lug83] LUGT H. J.: *Vortex flow in nature and technology*. Wiley, 1983. 1

[LVRL06] LI W.-C., VALLET B., RAY N., LEVY B.: Representing higher-order singularities in vector fields on piecewise linear surfaces. *IEEE Transactions on Visualization and Computer Graphics (Proc. IEEE Visualization) 12*, 5 (2006). 5

[MBES16] MACHADO G. M., BOBLEST S., ERTL T., SADLO F.: Space-time bifurcation lines for extraction of 2D Lagrangian coherent structures. *Computer Graphics Forum (Proc. EuroVis) 35*, 3 (2016), 91–100. 12

[MBS*04] MAHROUS K., BENNETT J., SCHEUERMANN G., HAMANN B., JOY K. I.: Topological segmentation in three-dimensional vector fields. *IEEE Transactions on Visualization and Computer Graphics 10*, 2 (2004), 198–205. 6

[MK85] MOIN P., KIM J.: The structure of the vorticity field in turbulent channel flow. Part 1. analysis of instantaneous fields and statistical correlations. *Journal of Fluid Mechanics 155* (1985), 441–464. 8, 15

[MK97] MIURA H., KIDA S.: Identification of tubular vortices in turbulence. *Journal of the Physical Society of Japan 66*, 5 (1997), 1331–1334. 8, 13

[MLP*10] MCLOUGHLIN T., LARAMEE R. S., PEIKERT R., POST F. H., CHEN M.: Over two decades of integration-based, geometric flow visualization. *Computer Graphics Forum 29*, 6 (September 2010), 1807–1829. 1

[Mof69] MOFFATT H. K.: The degree of knottedness of tangled vortex lines. *Journal of Fluid Mechanics 35*, 01 (1969), 117–129. 8, 10

[MPM*16] MARTINS R. S., PEREIRA A. S., MOMPEAN G., THAIS L., THOMPSON R. L.: An objective perspective for classic flow classification criteria. *Comptes Rendus Mecanique 344* (Jan. 2016), 52–59. 15

[MSE13] MACHADO G. M., SADLO F., ERTL T.: Local Extraction of Bifurcation Lines. In *Vision, Modeling and Visualization* (Lugano, Switzerland, 2013), The Eurographics Association, pp. 17–24. 12

[OJCJP16] OELTZE-JAFRA S., CEBRAL J. R., JANIGA G., PREIM B.: Cluster analysis of vortical flow in simulations of cerebral aneurysm hemodynamics. *IEEE Transactions on Visualization and Computer Graphics (Proc. IEEE Scientific Visualization 2015) 22*, 1 (2016), 757–766. 1

[Oku70] OKUBO A.: Horizontal dispersion of floatable particles in the vicinity of velocity singularities such as convergences. *Deep Sea Research and Oceanographic Abstracts 17*, 3 (1970), 445–454. 8, 10

[PC87] PERRY A. E., CHONG M. S.: A description of eddying motions and flow patterns using critical-point concepts. *Annual Review of Fluid Mechanics 19*, 1 (1987), 125–155. 12

[PC94] PERRY A. E., CHONG M. S.: Topology of flow patterns in vortex motions and turbulence. *Applied Scientific Research 53*, 3 (1994), 357–374. 17

[PKPH09] PETZ C., KASTEN J., PROHASKA S., HEGE H.-C.: Hierarchical vortex regions in swirling flow. *Computer Graphics Forum (Proc. EuroVis) 28*, 3 (2009), 863–870. 8, 11, 18

[Por98] PORTELA L. M.: *Identification and characterization of vortices in the turbulent boundary layer*. PhD thesis, Stanford University, 12 1998. 8, 9, 14

[POS*11] PAGOT C., OSMARI D., SADLO F., WEISKOPF D., ERTL T., COMBA J.: Efficient parallel vectors feature extraction from higher-order data. *Computer Graphics Forum (Proc. EuroVis) 30*, 3 (2011), 751–760. 6

[PPF*11] POBITZER A., PEIKERT R., FUCHS R., SCHINDLER B., KUHN A., THEISEL H., MATKOVIC K., HAUSER H.: The state of the art in topology-based visualization of unsteady flow. *Computer Graphics Forum 30*, 6 (2011), 1789–1811. 1, 6

[PR99] PEIKERT R., ROTH M.: The "parallel vectors" operator – a vector field visualization primitive. In *Proc. IEEE Visualization* (1999), pp. 263–270. 6, 11, 13, 14

[PVH*03] POST F. H., VROLIJK B., HAUSER H., LARAMEE R. S., DOLEISCH H.: The state of the art in flow visualisation: Feature extraction and tracking. *Computer Graphics Forum 22*, 4 (2003), 775–792. 1

[Rey94] REYNOLDS O.: On the dynamical theory of incompressible viscous fluids and the determination of the criterion. *Proceedings of the Royal Society of London 56*, 336-339 (1894), 40–45. 8, 17

[Rob90] ROBINSON S. K.: A review of vortex structures and associated coherent motions in turbulent boundary layers. In *Structure of Turbulence and Drag Reduction*. Springer, 1990, pp. 23–50. 8, 9

[Rob91] ROBINSON S. K.: Coherent motions in the turbulent boundary layer. *Annual Review of Fluid Mechanics 23*, 1 (1991), 601–639. 1, 6, 9, 15, 16

[Rot00] ROTH M.: *Automatic Extraction of Vortex Core Lines and Other Line-Type Features for Scientific Visualization*. Phd dissertation no. 13673, ETH Zürich, 2000. 12

[RP96] ROTH M., PEIKERT R.: Flow visualization for turbomachinery design. In *Proceedings of the 7th Conference on Visualization '96* (Los Alamitos, CA, USA, 1996), VIS '96, IEEE Computer Society Press, pp. 381–384. 1, 14

[RP98] ROTH M., PEIKERT R.: A higher-order method for finding vortex core lines. In *Proc. IEEE Visualization* (1998), pp. 143–150. 8, 11

[Sah09] SAHNER J.: *Extraction of Vortex Structures in 3D Flow Fields*. PhD thesis, University of Magdeburg, Germany, April 2009. 7

[SB90] SARKAR S., BALAKRISHNAN L.: Application of a Reynolds stress turbulence model to the compressible shear layer. In *21st Fluid Dynamics, Plasma Dynamics and Lasers Conference* (1990), p. 1465. 17

[SBV*11] SCHAFHITZEL T., BAYSAL K., VAARANIEMI M., RIST U., WEISKOPF D.: Visualizing the evolution and interaction of vortices and shear layers in time-dependent 3D flow. *IEEE Transactions on Visualization and Computer Graphics 17*, 4 (April 2011), 412–425. 19

[SH95] SUJUDI D., HAIMES R.: *Identification of Swirling Flow in 3D Vector Fields*. Tech. rep., Departement of Aeronautics and Astronautics, MIT, 1995. AIAA Paper 95-1715. 7, 8, 11, 12

[SH16a] SERRA M., HALLER G.: Forecasting long-lived Lagrangian vortices from their objective Eulerian footprints. *J. Fluid Mech.* (2016), to appear. 18

[SH16b] SERRA M., HALLER G.: Objective Eulerian coherent structures. *Chaos: An Interdisciplinary Journal of Nonlinear Science 26*, 5 (2016), 053110. 8, 18

[SKA99] STRAWN R. C., KENWRIGHT D. N., AHMAD J.: Computer visualization of vortex wake systems. *AIAA journal 37*, 4 (1999), 511–512. 8, 13, 16

[SKMR98] SCHEUERMANN G., KRUGER H., MENZEL M., ROCKWOOD A.: Visualizing nonlinear vector field topology. *IEEE Transactions on Visualization and Computer Graphics 4*, 2 (1998), 109–116. 5

[SOK*13] SHAFII S., OBERMAIER H., KOLÁŘ V., HLAWITSCHKA M., GARTH C., HAMANN B., JOY K. I.: Illustrative rendering of vortex cores. In *Eurographics Conference on Visualization (EuroVis 2013) Short Papers* (Leipzig, Germany, 2013), pp. 61–65. 19

[SP99] SADARJOEN I. A., POST F. H.: Geometric methods for vortex extraction. In *Data Visualization '99*, Eurographics. Springer Vienna, 1999, pp. 53–62. 8, 14, 19

[SP00] SADARJOEN I. A., POST F. H.: Detection, quantification, and tracking of vortices using streamline geometry. *Computers and Graphics 24*, 3 (2000), 333–341. 14

[SPP04] SADLO F., PEIKERT R., PARKINSON E.: Vorticity based flow analysis and visualization for Pelton turbine design optimization. In *Proc. IEEE Visualization* (2004), pp. 179–186. 9, 15

[SPS06] SADLO F., PEIKERT R., SICK M.: Visualization tools for vorticity transport analysis in incompressible flow. *IEEE Transactions on Visualization and Computer Graphics 12*, 5 (2006), 949–956. 19

[ST05] SCHEUERMANN G., TRICOCHE X.: Topological methods for flow. *The Visualization Handbook* (2005), 341. 4, 6

[STH*09] SHI K., THEISEL H., HAUSER H., WEINKAUF T., MATKOVIC K., HEGE H.-C., SEIDEL H.-P.: Path line attributes - an information visualization approach to analyzing the dynamic behavior of 3D time-dependent flow fields. In *Topology-Based Methods in Visualization II*, Mathematics and Visualization. Springer, 2009, pp. 75–88. 8, 15

[SVG*08] SCHAFHITZEL T., VOLLRATH J., GOIS J., WEISKOPF D., CASTELO A., ERTL T.: Topology-preserving lambda2-based vortex core line detection for flow visualization. *Computer Graphics Forum (Proc. EuroVis) 27*, 3 (2008), 1023–1030. 8, 13

[SWH05a] SAHNER J., WEINKAUF T., HEGE H.-C.: Galilean invariant extraction and iconic representation of vortex core lines. In *Proc. Eurographics / IEEE VGTC Symposium on Visualization (EuroVis)* (Leeds, United Kingdom, 2005), pp. 151–160. 8, 13, 19

[SWH05b] STALLING D., WESTERHOFF M., HEGE H.-C.: Amira: A highly interactive system for visual data analysis. In *The Visualization Handbook*. Elsevier, 2005, pp. 749–767. 20

[SWTH07] SAHNER J., WEINKAUF T., TEUBER N., HEGE H.-C.: Vortex and strain skeletons in Eulerian and Lagrangian frames. *IEEE Transactions on Visualization and Computer Graphics 13*, 5 (2007), 980–990. 8, 13, 14, 15, 16

[The02] THEISEL H.: Designing 2D vector fields of arbitrary topology. *Computer Graphics Forum (Proc. Eurographics) 21*, 3 (2002), 595–604. 4, 5

[Tho08] THOMPSON R. L.: Some perspectives on the dynamic history of a material element. *International Journal of Engineering Science 46*, 3 (2008), 224–249. 15

[TK94] TABOR M., KLAPPER I.: Stretching and alignment in chaotic and turbulent flows. *Chaos, Solitons & Fractals 4*, 6 (1994), 1031–1055. 8, 15

[TLHD03] TONG Y., LOMBEYDA S., HIRANI A. N., DESBRUN M.: Discrete multiscale vector field decomposition. *ACM Trans. Graph. (Proc. SIGGRAPH) 22*, 3 (2003), 445–452. 8, 17

[TN65] TRUESDELL C., NOLL W.: *The nonlinear field theories of mechanics*. Handbuch der Physik, Band III/3, e by Flugge, S., (ed.) , Springer-Verlag, Berlin, 1965. 7

[TRS03] THEISEL H., RÖSSL C., SEIDEL H.-P.: Compression of 2D vector fields under guaranteed topology preservation. *Computer Graphics Forum (Proc. Eurographics) 22*, 3 (2003), 333–342. 4

[Tru53] TRUESDELL C.: Two measures of vorticity. *J. Rational Mech. and Analysis 2* (1953), 173–217. 8, 10

[TS03] THEISEL H., SEIDEL H.-P.: Feature flow fields. In *Proc. Symposium on Data Visualisation* (Grenoble, France, 2003), pp. 141–148. 4, 5, 13

[TSH00] TRICOCHE X., SCHEUERMANN G., HAGEN H.: A topology simplification method for 2D vector fields. In *Proc. Visualization* (Salt Lake City, Utah, USA, Oct 2000), pp. 359–366. 4, 5

[TSW*05] THEISEL H., SAHNER J., WEINKAUF T., HEGE H.-C., SEIDEL H.-P.: Extraction of parallel vector surfaces in 3D time-dependent fields and application to vortex core line tracking. In *Proc. IEEE Visualization* (Minneapolis, Minnesota, USA, 2005), pp. 631–638. 8, 12

[TWHS03] THEISEL H., WEINKAUF T., HEGE H.-C., SEIDEL H.-P.: Saddle connectors - an approach to visualizing the topological skeleton of complex 3D vector fields. In *Proc. IEEE Visualization* (Seattle, Washington, USA, 2003), pp. 225–232. 5

[TWHS04] THEISEL H., WEINKAUF T., HEGE H.-C., SEIDEL H.-P.: Grid-independent detection of closed stream lines in 2D vector fields. In *Proc. Vision, Modeling and Visualization* (Stanford, California, USA, November 2004), pp. 421–428. 5, 8, 14

[TWSH02] TRICOCHE X., WISCHGOLL T., SCHEUERMANN G., HAGEN H.: Topology tracking for the visualization of time-dependent two-dimensional flows. *Computers & Graphics 26*, 2 (2002), 249–257. 12, 18

[VG12] VAN GELDER A.: Vortex core detection: Back to basics. In *IS&T/SPIE Electronic Imaging* (Burlingame, California, USA, 2012), International Society for Optics and Photonics, pp. 829413–829413. 14

[VGP09] VAN GELDER A., PANG A.: Using PVsolve to analyze and locate positions of parallel vectors. *IEEE Transactions on Visualization and Computer Graphics 15*, 4 (2009), 682–695. 6

[VV92] VILLASENOR J., VINCENT A.: An algorithm for space recognition and time tracking of vorticity tubes in turbulence. *CVGIP: Image Understanding 55*, 1 (1992), 27 – 35. 8, 14

[WCW*09] WIEBEL A., CHAN R., WOLF C., ROBITZKI A., STEVENS A., SCHEUERMANN G.: Topological flow structures in a mathematical model for rotation-mediated cell aggregation. *Topological Data Analysis and Visualization: Theory, Algorithms and Applications* (2009), 1–12. 8, 14

[Wei91] WEISS J.: The dynamics of enstrophy transfer in two-dimensional hydrodynamics. *Physica D: Nonlinear Phenomena 48*, 2-3 (1991), 273–294. 8, 10

[Wei08] WEINKAUF T.: *Extraction of Topological Structures in 2D and 3D Vector Fields*. PhD thesis, University Magdeburg, 2008. 3, 4, 6

[Wie04] WIEBEL A.: *Feature Detection in Vector Fields Using the Helmholtz-Hodge Decomposition*. Diploma thesis, Univ. Kaiserslautern, 2004. 17

[WJE01] WESTERMANN R., JOHNSON C., ERTL T.: Topology-preserving smoothing of vector fields. *IEEE Transactions on Visualization and Computer Graphics 7*, 3 (2001), 222–229. 4

[WS01] WISCHGOLL T., SCHEUERMANN G.: Detection and visualization of closed streamlines in planar flows. *IEEE Transactions on Visualization and Computer Graphics 7*, 2 (2001), 165–172. 5, 8, 14

[WSH01] WISCHGOLL T., SCHEUERMANN G., HAGEN H.: Tracking closed streamlines in time dependent planar flows. In *Proceedings of Vision, Modeling and Visualization* (Stuttgart, Germany, 2001), pp. 447–454. 18

[WSTH07] WEINKAUF T., SAHNER J., THEISEL H., HEGE H.-C.: Cores of swirling particle motion in unsteady flows. *IEEE Transactions on Visualization and Computer Graphics (Proc. Visualization) 13*, 6 (2007), 1759–1766. 4, 6, 7, 8, 11, 12, 13, 17, 19

[WT10] WEINKAUF T., THEISEL H.: Streak lines as tangent curves of a derived vector field. *IEEE Transactions on Visualization and Computer Graphics (Proc. Visualization) 16*, 6 (2010), 1225–1234. 8, 14, 15

[WTGP11] WEINKAUF T., THEISEL H., GELDER A. V., PANG A.: Stable feature flow fields. *IEEE Transactions on Visualization and Computer Graphics 17*, 6 (2011), 770–780. 5, 6

[WTHS04a] WEINKAUF T., THEISEL H., HEGE H.-C., SEIDEL H.-P.: Boundary switch connectors for topological visualization of complex 3D vector fields. In *Proc. Symposium on Data Visualisation (VISSYM)* (Konstanz, Germany, 2004), pp. 183–192. 6

[WTHS04b] WEINKAUF T., THEISEL H., HEGE H.-C., SEIDEL H.-P.: Topological construction and visualization of higher order 3D vector fields. *Computer Graphics Forum (Proc. Eurographics) 23*, 3 (2004), 469–478. 4

[WTHS06] WEINKAUF T., THEISEL H., HEGE H.-C., SEIDEL H.-P.: Topological structures in two-parameter-dependent 2D vector fields. *Computer Graphics Forum (Proc. Eurographics) 25*, 3 (2006), 607–616. 6

[XXLL10] XIE C., XING L., LIU C., LI X.: *Multi-scale Vortex Extraction of Ocean Flow*. Springer US, Boston, MA, 2010, pp. 173–183. 5, 8, 14

[ZABK99] ZHOU J., ADRIAN R. J., BALACHANDAR S., KENDALL T. M.: Mechanisms for generating coherent packets of hairpin vortices in channel flow. *Journal of Fluid Mechanics 387* (1999), 353–396. 8, 9, 10